NUMERICAL MODELLING OF SPATIO-TEMPORAL PATTERNS IN A DC-DRIVEN GAS DISCHARGE-SEMICONDUCTOR SYSTEM

A THESIS SUBMITTED TO
THE GRADUATE SCHOOL OF APPLIED MATHEMATICS
OF
MIDDLE EAST TECHNICAL UNIVERSITY
BY

GÖZDE ÖZDEN

IN PARTIAL FULFILLMENT OF THE REQUIREMENTS
FOR
THE DEGREE OF MASTER OF SCIENCE
IN
SCIENTIFIC COMPUTING

SEPTEMBER 2015

Approval of the thesis:

NUMERICAL MODELLING OF SPATIO-TEMPORAL PATTERNS IN A DC-DRIVEN GAS DISCHARGE-SEMICONDUCTOR SYSTEM

submitted by **GÖZDE ÖZDEN** in partial fulfillment of the requirements for the degree of **Master of Science in Scientific Computing Program, Middle East Technical University** by,

Prof. Dr. Bülent Karasözen _____
Director, Graduate School of **Applied Mathematics**

Assoc. Prof. Dr. Ömür Uğur _____
Head of Department, **Scientific Computing**

Assoc. Prof. Dr. İsmail Rafatov _____
Supervisor, **Department of Physics, METU**

Prof. Dr. Bülent Karasözen _____
Co-supervisor, **Institue of Applied Mathematics, METU**

Examining Committee Members:

Assoc. Prof. Dr. Serhat Çakır _____
Department of Physics, METU

Assoc. Prof. Dr. İsmail Rafatov _____
Department of Physics, METU

Prof. Dr. Bülent Karasözen _____
Institue of Applied Mathematics, METU

Assoc. Prof. Dr. Alpan Bek _____
Department of Physics, METU

Assoc. Prof. Dr. Hüseyin Oymak _____
Physics Group, Atılım University

Date: _____

I hereby declare that all information in this document has been obtained and presented in accordance with academic rules and ethical conduct. I also declare that, as required by these rules and conduct, I have fully cited and referenced all material and results that are not original to this work.

Name, Last Name: GÖZDE ÖZDEN

Signature :

ABSTRACT

NUMERICAL MODELLING OF SPATIO-TEMPORAL PATTERNS IN A DC-DRIVEN GAS DISCHARGE-SEMICONDUCTOR SYSTEM

ÖZDEN, GÖZDE

M.S., Department of Scientific Computing

Supervisor : Assoc. Prof. Dr. İsmail Rafatov

Co-Supervisor : Prof. Dr. Bülent Karasözen

SEPTEMBER 2015, 44 pages

In this thesis, numerical modelling of temporal and spatial pattern formation in the planar layered system, consisted of a DC driven planar gas discharge layer, coupled to high ohmic semiconductor layer, is carried out in 1D and 2D Cartesian geometry. Numerical model includes continuity equations for ions and electrons, the Poisson equation for the electric field, the energy balance equation for the background gas. The conditions correspond to a transition from the Townsend regime to the glow discharge. Calculations are performed for the nitrogen at medium pressure, using Comsol Multiphysics and Matlab packages. First, period doubling bifurcation of the system is observed within 1D model and related Lorenz maps are derived. Then, stable pattern formation is studied within 2D model. The effects of different modeling approaches, including the effect of heating of the background gas, is examined.

Keywords: plasma, gas discharge, barrier discharge, nonlinear dynamics, pattern formation

ÖZ

DC GAZ DEŞARJI-YARI İLETKEN SİSTEMDEKİ UZAY-ZAMANSAL YAPININ NÜMERİK MODELLENMESİ

ÖZDEN, GÖZDE

Yüksek Lisans, Bilimsel Hesaplama Bölümü

Tez Yöneticisi : Doç. Dr. İsmail Rafatov

Ortak Tez Yöneticisi : Prof. Dr. Bülent Karasözen

Eylül 2015 , 44 sayfa

Bu tezde yüksek dirençli yarı iletken tabaka ile birleştirilmiş DC güdümlü düzlemsel deşarj katmanını içeren sistemde uzay-zamansal yapının oluşumunun nümerik modellenmesi 1 ve 2 boyutlu olarak kartezyen geometride çalışılmıştır. Nümerik model, iyonlar ve elektronlar için süreklilik denklemlerini, elektrik alan için Poisson denklemini, arka plandaki gaz için enerji denge denklemini içerir. Durumlar Townsend rejimden glow deşarja geçişe karşılık gelir. Hesaplamalar orta basınçlı nitrojen için Comsol Multiphysics ve Matlab paketleri kullanılarak yapılmıştır. İlk olarak, sistemin periyodunun ikiye katlanmasındaki çatallanma 1 boyutlu gözlenmiştir ve Lorenz çizimi uygulanmıştır. Daha sonra, durgun yapı oluşumu 2 boyutlu modelde çalışılmıştır. Çeşitli arka plan gaz sıcaklığında, değişik model yaklaşımlarının etkisi incelenmiştir.

Anahtar Kelimeler: plazma, gaz deşarjı, bariyer deşarjı, doğrusal olmayan dinamikler, pattern oluşumu

to my family

ACKNOWLEDGMENTS

First of all, I would like to thank my supervisor Assoc. Prof. Dr. İsmail Rafatov for guiding me through my graduate study and for his patience.

I owe special thanks my co-supervisor Prof. Dr. Bülent Karasözen who gave me huge support to begin this thesis.

My sincere thanks also goes to Assoc. Prof. Serhat Çakır for giving me the opportunity to join research group at the Department of Physics and for encouraging me.

I would like to thank Ender Eylenceoğlu for stimulating discussions.

Last but not the least, I would like to Yakup Hafızoğlu for supporting me spiritually throughout writing this thesis.

TABLE OF CONTENTS

LIST OF TABLES

TABLES

LIST OF FIGURES

FIGURES

LIST OF ABBREVIATIONS

1D	1-Dimensional
2D	2-Dimaensional
DBD	Dielectric Barrier Discharge
FDM	Finite Difference Method
FEM	Finite Element Method
GDG	Gas Discharge Gap
SC	Semiconductor

CHAPTER 1

INTRODUCTION

One of the main problems in philosophy and science is the existence and origin of order. It was believed that ordered patterns and structures are created with the external intervention or control. In the last couple of decades, the problem has been categorized into the context of self-organization.

It is self-evident the importance of the pattern and form in biology since it is impossible not to see these patterns in the animal world. In Figure 1.1, only two examples are given. The process is still unknown because of lack of inclusion genes in the models and lack of translation genetic information into physical systems [1, 2].

(a) zebras (b) a leopard

Figure 1.1: Examples of pattern in animal world [3].

These patterns are observed in reaction diffusion systems such as granular media, lasers, reacting chemicals and especially plasma. Figure 1.2 demonstrate only two results of the experiment done by Gunaratne and his group in 1994. In this experiment, chorite-iodide-malonic acid was used as a reaction diffusion system. Transition stripe to hexagone type of these patterns were observed with this experiment [1].

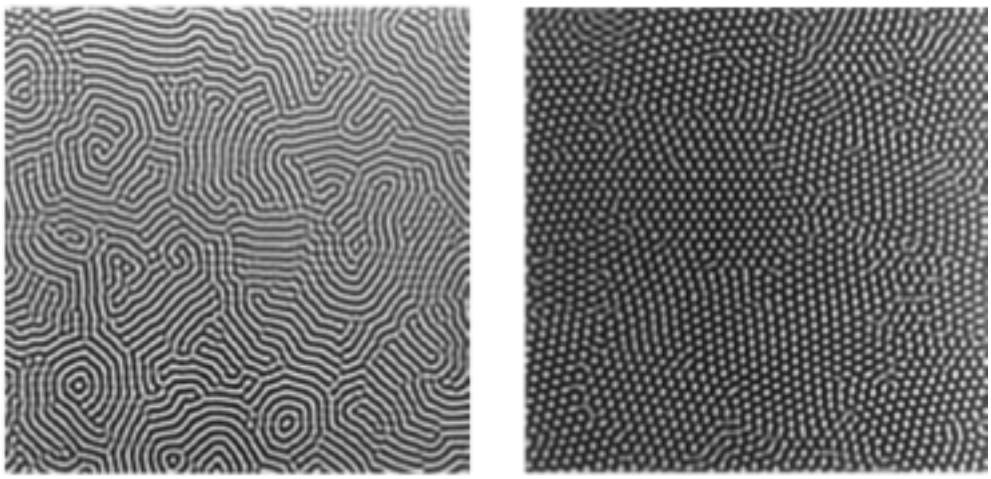

Figure 1.2: Stripe and hexagone structures by chlorite-iodide-malonic reaction diffusion system [1].

It is known from many numerical studies that steady state finite amplitude spatial patterns can be produced by reaction diffusion systems. Such patterns are called as Turing patterns. Turing implied that chemicals can react and diffuse in such a way as to produce steady state heterogeneous spatial patterns of chemical under certain conditions [4]. These reaction diffusion systems are described with nonlinear differential equations in the form:

$$\frac{\partial c}{\partial t} = f(c) + D\nabla^2 c. \tag{1.1}$$

where c is the concentration, f is reaction function and D is the diffusion coefficient [1].

This type of equations can not be solved analytically due to the absence of general methods for solving them. In this case, it is used some numerical techniques such as FEM and FDM.

In the last couple of decades, electrical systems are also defined as reaction diffusion types. Experimentally, different type of patterns were obtained as shown in Figure 1.3. These patterns were obtained increasing the applied voltage value in the same experiment. In this experiment, SC-GDG system was used. Two different resistivity of the SC is used as an electrode. Transition to different structures in the following order hexagone, stripe and stripe with defect were obtained.

In this thesis work, SC-GDG system is studied numerically to understand the pattern formation.

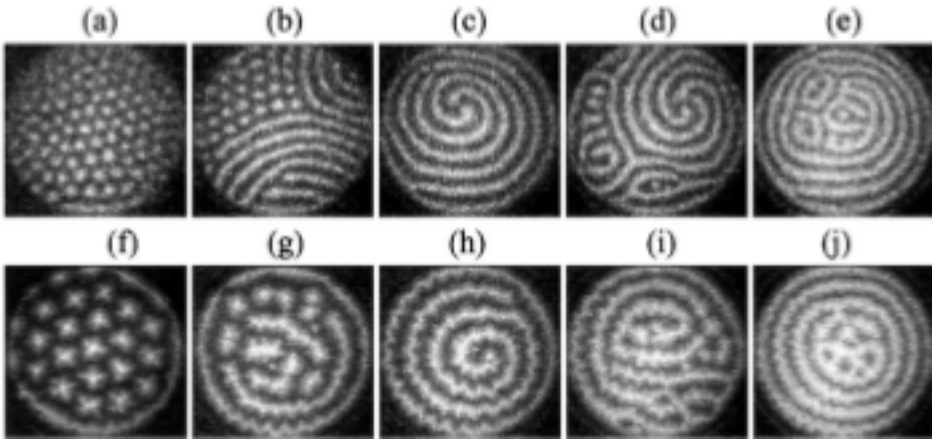

Figure 1.3: Sequence of snapshots (a)-(e) and (f)-(j) obtained by two different resistivity of the SC (1.6×10^9 Ωcm and 3.5×10^8 Ωcm),$p = 11.25$ Torr, $T = 90$ K [5].

1.1 Gas Discharge

Gas discharge physics deals with the flow of the current through the ionized gas. When the gas at appropriate pressure in a gap between electrodes is exposed to an applied electric field, discharge occurs. The process occurs inside small tube as shown in Figure 1.4. There are two parallel electrodes. They are connected to the power supply. It is filled with gas. If the pressure inside the tube is sufficient, the process occurs applying sufficient voltage.

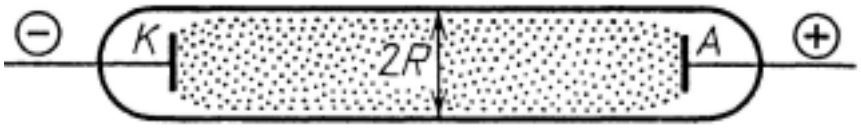

Figure 1.4: A gas discharge tube [6].

There are many types of discharge. They can be divided into two main categorizes. One of them is non-self-sustaning. In this type, current growth depends on the limitted rate of ionization as increasing the voltage. This means that external source is necessary to ionize the molecules since electrons can not continue the process. The other one is self-sustaining ionization. In this case, electrons are produced by incident radiation at the cathode. They gain the energy in the field. They cause the ionization to consume this extra energy. Then, the process occurs.

Self-sustaining discharge includes many important types such as glow discharge, Townsend discharge and arc discharge. They differ from each other in the current and applied voltage [6].

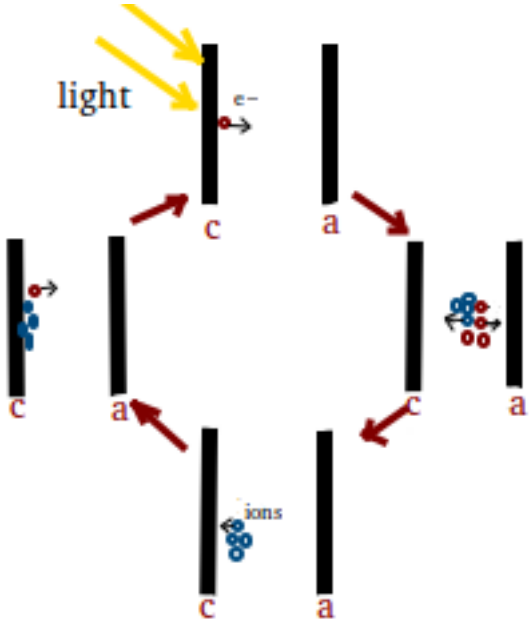

Figure 1.5: Schematic diagram of Townsend ionization.

1.2 Townsend Ionzation and Electric Breakdown

In genereal, the process of transformation of a nonconducting material into a conducting applying to it a sufficiently strong field is defined as electric breakdown. In this process, Townsend ionization occurs. A few electrons initiates the avalanche multiplying accidentally due to incident radiation such as cosmic rays and photoelectrons that is produced by cathode irradiated by a ultraviolet light. Then, energy increases in the field. Thus, these electrons ionize gas molecules to consume this extra energy and new electrons and molecules are produced. Accelerating these electrons in the field, the process occurs again. Then, these produced positively ions bombard the cathode and new electrons are moves to the anode again. This process is called secondary emission or γ process [6],[2].

In Figure 1.5, this process is shown for only one electron. When the light fall into cathode, the electron is emitted. This electron moves to the anode, opposite direction of the electric field, and molecules are ionized. Positively charged molecules, ions, arrive the cathode and this process occur again producing electron picking up from the cathode after bombardment of the ions.

Mathematically, taking n as the number of electrons produced by one electron in a discharge gap with lenght d (assuming larger than the mean free path of an electron, λ_f)

$$\frac{dn}{dx} = \alpha n, \tag{1.2}$$

α is the first ionization coefficient, n_0 is the number of emitted electrons. Then, n yields

$$n = n_0 e^{\alpha x}. \tag{1.3}$$

Then, the current in the gap is

$$i = en_0 e^{\alpha x}. \tag{1.4}$$

The number of ions is

$$n_i = \gamma n_0 [e^{\alpha x} - 1], \tag{1.5}$$

where γ is the secondary emission coefficeint for the cathode. Then, the breakdown condition can be obtained from n and n_i as

$$e^{\alpha x} = 1 + \frac{1}{\gamma}. \tag{1.6}$$

The electric field on the cathode is ratio of the electric potential to the discharge gap, $E = V/d$ where V is the applied voltage. Thus, λ_f must be smaller than $d = V/E$ and probability of it is $exp(-x/\lambda_f)$. Townsend coefficent is defined as the number of collisions leading to ionizations per unit length. It is

$$\alpha = Ape^{-Bp/E}, \tag{1.7}$$

$$\alpha x = \ln(1 + 1/\gamma). \tag{1.8}$$

Here, $A = 1/\lambda_f$ and $B = V/\lambda_f$. These constants depend on the gas species and they are obtained from experimental results [6]. p is the reduced pressure.

Putting these coefficents into breakdown condition defined by equation (1.8), breakdown voltage V_t is

$$V_t = \frac{B(px)}{In(\frac{A}{In(1/\gamma)+1}) + In(px)}, \quad \frac{E}{p} = \frac{B}{In(\frac{Apx}{In(1+1/\gamma)})}. \tag{1.9}$$

Characteristic value of the current corresponding Townsend discharge is [6, 7]

$$J_c = \frac{\epsilon_0 \mu_i V_t^2}{2x^3}, \tag{1.10}$$

where μ_i is the mobility coefficeint for the ions.

1.3 Dielectric Barrier Discharge

DBD systems consist of two parellel electrodes one of them covered with dielectric layer. The experimental setup is similar with SC-DGD systems as shown in Figure 1.6. Electrodes are transparant to observe the spatial distribution of the patterns. This type is commonly used in research [8] and it is important since the first observation of pattern formation was performed on DBD system by Boyers and Tiller at 1982 [9]. 50 μm gas tube filed with He gas at atmospheric pressure in that work. Hexagonal array of current filaments were obtained. Increasing the applied voltage, the structure of filaments turned into stripes [2].

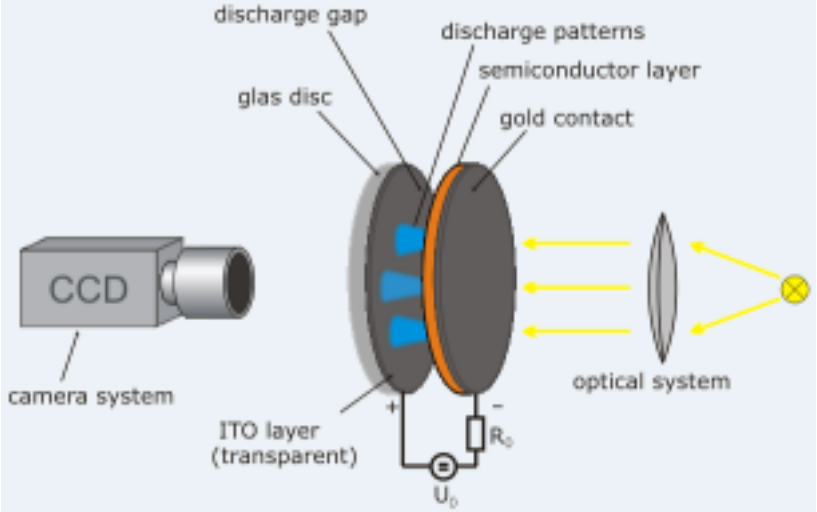

Figure 1.6: SC-GDG system experimental setup [14].

1.4 Aims and Motivations

Gas discharge is a complicated system since it is affected from a lot of parameters. These parameters are gas species, pressure, temperature, applied voltage (AC or DC) and so on [10]. Semiconductor-gas discharge gap (SC-GDG) systems is one of the great example of the gas discharge field. In this case, semiconductor is used as the cathod and it is made of high Ohmic material such as gallium arsenide (GaAs) and silicon (Si). In these systems, current could not increase so high since the semiconductor with high Ohmic character does not allow to occur.

Arising of the patterns is explained in different perspective of the view. One of the most attained view is current-voltage characteristic (CVC) issue. According to it, it is predicted transition from Townsend discharge to glow discharge [11]. It is defined as glow discharge is appeared in $100 - 1000$ V voltage getting low current as 0.1 A - 1 μA [6].

In present work, SC-GDG system under cryogenic conditions is shown. In this case, DC voltage is applied. The current is approximately$1 - 10$ μA/cm^2. This value is a quite small but it appears due to high Ohmic resistance of the semiconductor. This kind of discharge is known as Townsend discharge [7]. In this case, temperature is below 123 K to get the current with that value. Under that conditions, patterns can be obtained. If the temperature increases, the current increases so patterns can disappear.

In order to understand the mechanism of the pattern formation, some experimental works were done in the past. Some of the primary works were done H.G. Purwins, A. Astrov and E. Ammelt in the mid of the 1990s [12, 5]. In these works, SC-GDG system is used and different type of patterns were obtained namely spiral, target and hexagonal. These patterns appeared in transition between each other by changing some conditions, especially applied voltage. The main interest is how patterns appear and in which conditions they change.

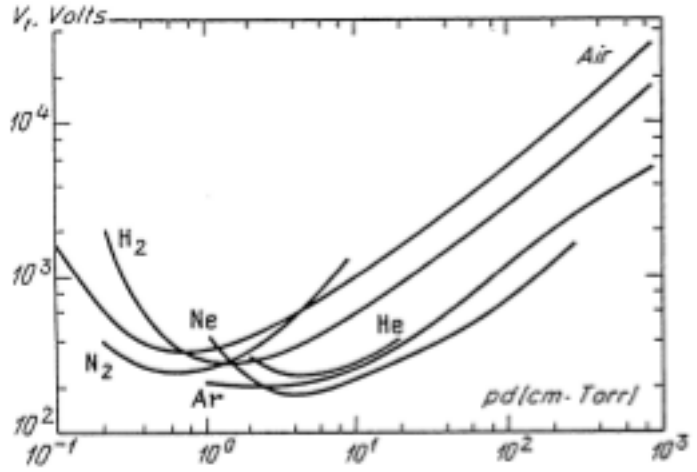

Figure 1.7: Breakdown potentials in various gases (Paschen curve) [6].

The system is similar with one that was used by Prof. Dr. H.G. Purwins and his group one [8, 13] shown in Figure 1.6. There are discharge gap and semiconductor layer. By the camera system, these patterns can be recorded. By doing this, theory can be compared with the experimental results. In our case, the diameter of the discharge area is 2 cm. The thickness of the discharge gap is $d = 0.044$ cm and it is $d_s = 0.1$ cm for the semiconductor layer. Discharge gap is filled with nitrogen gas with presure 211.52 Torr. Its reduced pressure is $p = 619.8$ Torr so the value of $pd \approx 27.3$ gives that discharge occurs right side of the Paschen curve. It is important to understand the formation of the patterns. It was implied that patterns appear due to the heating of the gas by the discharge current [7]. It is known as a thermal mechanism. This mechanism causes the pattern formation since discharge conditions belong to the right side of the Paschen's curve which is shown in Figure 1.7. When the heat increases at a fixed place, the gas expands so its density decreases. This causes the voltage decline and so discharge occurs.

Parameters are taken from the experiment which was done before [7, 13]. It is important to define the model and the physical system in order to understand the process. Figure 1.6 demonstrate the experimental setup.

The system is shown schematically in Figure-1.8. It is seperated into two parts. Lowest part of the system is the gas discharge gap (GDG). It is filled with nitrojen. Semiconductor is in the upper part. In the GDG, electrons and ions act due to electric field formed from potential. Electrons appear by the collison of the positively charged ions with the cathode. This process is called γ-process as explained in the introduction chapter. Electrons appear as a result of this process. This is known as α- process.

Gas discharge occurs following these two processes each other in simply. The current is expected to be low since resistance of the conductor is very high. When the applied voltage changes a litte, structure turns into another one. For example, hexagon patterns occur about 1815 V and it turns into stripe structure

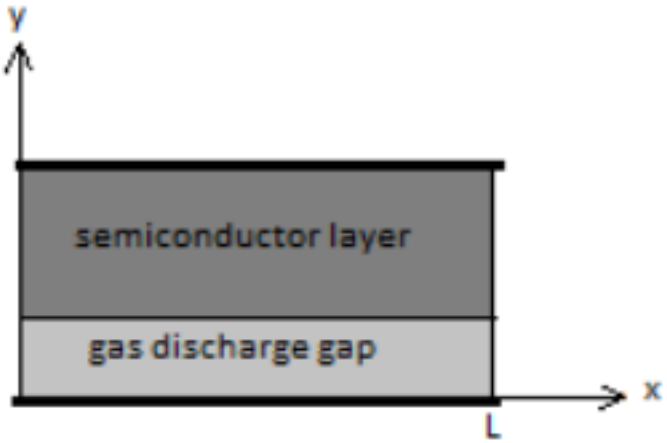

Figure 1.8: Schematic diagram of the SC-GDG system.

about 1935 V [10]. Here, hexagon type is discussed. In Figure 1.9, the experimental result of this work is shown [7]. The image was recorded with the camera.

Formation of pattern structures are generally explained by current-voltage char-

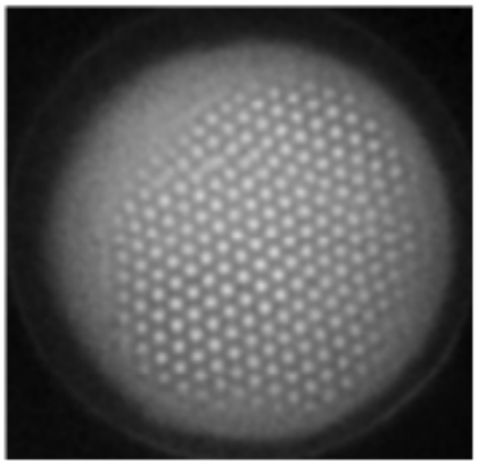

Figure 1.9: Hexagonal current patterns [7], $p = 211.52$ Torr, $T = 100$ K $U_t = 2400$ V.

acteristic (CVC) [16]. However, this approximation is valid for higher current density [17]. In this case, the current density is in the micro range. Thus, it is necessary to insert new terms to the model in order to explain the formation of the structures. Thermal conductivity equation covers this addition [7].

1.5 Organization of the Thesis

In Chapter 2, equations of the SC-GDG model are introduced. These equations are continuity equation for particle species, Poisson equation for electric

field, and heat equation for the background gas. Then, boundary conditions are defined for 1D and 2D cases. Dimensional analysis is done in following part. Next, equations are derived using adiabatic elimination of electrons. The main aim is to show that solutions can be obtained using the tricks belonging this method. Then, parameter regime is given. Data in that part are taken from experimental and theoretical works [15, 7]. Calculations were perfomed on the package namely COMSOL®.

In Chapter 3, results are discussed. Firstly, 1D results of the system were demonstrated in order to show the validity of the model. Then, Lorenz map was plotted to show a transition to the chaotic state. Next, 1D system solutions in there different cases are compared. If there is any difference between them, effects of control parameters in each cases is discussed. Then, the solutions that was obtained by adiabatic elimination method. Effect of this method is discussed. Next, solutions that are obtained with Scharfetter Gummel method are compared with others. 2D solutions are mentioned.

In Chapter 5, whole results are summarized and they are compared with the literature. Then, potential future works are discussed.

CHAPTER 2

THE SC-GDG MODEL

2.1 Derivation of Equations

Consider a differential element of surface as shown in Figure 2.1. It is centered at the point $\mathbf{x}(t) = (x, y)$ at time t. As shown on this figure, $\mathbf{u}$ is the mean velocity of particle species with density n. The number of particles flowing across the surface, $n\mathbf{u}dxdy$, changes with time as follows,

$$\frac{\partial n}{\partial t}dxdy = -[n\mathbf{u}_x dy]_{x+dx} + [n\mathbf{u}_x dy]_x - [n\mathbf{u}_y dx]_{y+dy} + [n\mathbf{u}_y dx]_y. \tag{2.1}$$

Indexes on the velocity imply the direction of it. If it is divided by surface area,

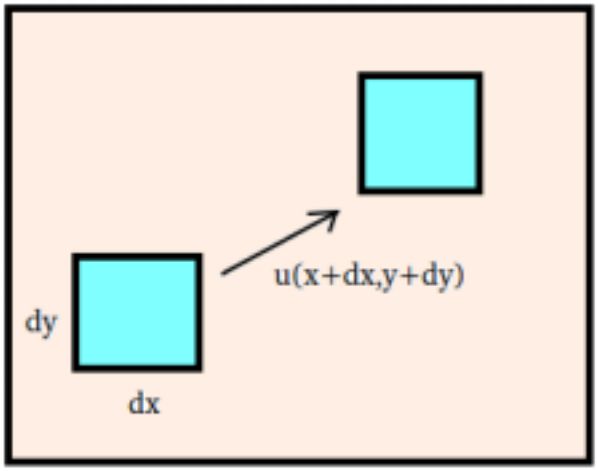

Figure 2.1: Small particle moving with velocity $\mathbf{u}$.

$dxdy$, the well known continuity equation is obtained,

$$\frac{\partial n}{\partial t} = -\frac{\partial}{\partial x}(n\mathbf{u}_x) - \frac{\partial}{\partial y}(n\mathbf{u}_y). \tag{2.2}$$

Then, if the source term, S, is added for the collisional case, the continuity equation can be written as, [18],

$$\frac{\partial n}{\partial t} + \nabla \cdot \mathbf{\Gamma} = S. \tag{2.3}$$

Here, $\mathbf{\Gamma} = n\mathbf{u}$ is the particle flux. Then, the equation of motion of the particle, [6, 18], is

$$m\frac{\partial \mathbf{u}}{\partial t} = q\mathbf{E} - \nabla p. \tag{2.4}$$

where m is the mass of the particle, q is the charge of the particle, ν is the collision frequency, index i implies the ith collision, gradient term denotes the change in the velocity and p is the pressure. Using $p = kTn$, integration of the equation (2.4) yields,

$$\mathbf{u} = \frac{q}{m\nu}\mathbf{E} - \frac{kT}{m\nu}\frac{\nabla n}{n}. \tag{2.5}$$

Here, k is the Boltzmann constant, T is the temperature and ν is the collision frequency. The coefficient of the electric field is called as mobility and the other term is called diffusion

$$\mu = \frac{q}{m\nu}, \qquad D = \frac{kT}{nm\nu}. \tag{2.6}$$

There is a relation between these two coefficients $\mu = |q|D/(kT)$, called Einstein relation [6]. Then, partical flux is

$$\mathbf{\Gamma} = -\mu n\mathbf{E} - D\nabla n. \tag{2.7}$$

For two fluid plasma of ions and electrons, it must be defined two different fluxes as

$$\mathbf{\Gamma}_e = -\mu_e n_e\mathbf{E} - D_e\nabla n_e, \quad \mathbf{\Gamma}_i = \mu_i n_i\mathbf{E} - D_i\nabla n_i. \tag{2.8}$$

Subscripts e and i denotes the electron and ion species.

The mean velocity in equation (2.5) includes two terms, namely drift and diffusion. The drift term is $v_d = \mu\mathbf{E}$. The mobility and collision frequency are assumed to be constant in the analysis [6]. The frequency in this term is proportional to the gas pressure. Thus, the drift velocity is proportional with the ratio $|\mathbf{E}|/p$. It depends on the combination of reduced $|\mathbf{E}|/p$, not individually $\mathbf{E}$ and p [6].

The right hand side in equation (2.3) implies the source term. Physical meaning of it is explained in the introduction chapter as ionization process. This term can be arised by creation of particles or decreation by loss of particles [18]. In the source term, classical Townsend approximation is used [6]. According to this approximation, the coefficient is defined as

$$\alpha(|\mathbf{E}|/E_0) = e^{(-E_0/\mathbf{E})}. \tag{2.9}$$

In this term, E_0 is proportional with the reduced pressure in this model. In this work, ionization is taken into account, but recombination which is the charge decay process is neglected. Thus, the source term is written as a sum of generation by impact ionization in Townsend approximaton [16],

$$S = |-\mu_e n_e\mathbf{E} - D_e\nabla n_e|\bar{\alpha}(|\mathbf{E}|), \quad \bar{\alpha}(|\mathbf{E}|) = \alpha_0\alpha\left(\frac{|\mathbf{E}|}{E_0}\right). \tag{2.10}$$

The continuity equation is used to define the each charge particle density in the system. These particles are electrons and ions. These equations are written as

$$\frac{\partial n_e}{\partial t} + \nabla \cdot (-\mu_e n_e \mathbf{E} - D_e \nabla n_e) = |-\mu_e n_e \mathbf{E} - D_e \nabla n_e| \, \bar{\alpha}(|\mathbf{E}|), \tag{2.11}$$

$$\frac{\partial n_i}{\partial t} + \nabla \cdot (\mu_i n_i \mathbf{E} - D_i \nabla n_i) = |-\mu_e n_e \mathbf{E} - D_e \nabla n_e| \, \bar{\alpha}(|\mathbf{E}|). \tag{2.12}$$

The subscript g refers to the gas discharge region and s refers to semiconductor region. Poisson equation is used to get the solution of the electric field in GDG,

$$\nabla \cdot \mathbf{E} = \frac{e}{\epsilon_0}(n_i - n_e), \quad \mathbf{E} = -\nabla \varphi_g. \tag{2.13}$$

Here, e is the electric charge, ϵ_0 is the dielecric constant of the vacuum, φ_g is the electric potential in the GDG region. The electric field in the SC region can be calculated using current density which is

$$\alpha(|\mathbf{E}|/E_0) = exp(-E_0/\mathbf{E}), \quad \nabla \cdot \mathbf{J}_s = 0. \tag{2.14}$$

Here, $\bar{\sigma_s}$ is the conductivity of the semiconductor. Its value is constant and it is a property that changes matter to matter. φ_s is the potential on the SC area and it is interested in the stationary solution so

$$\nabla \cdot \mathbf{E} = 0, \quad \mathbf{E} = -\nabla \varphi_s. \tag{2.15}$$

Using particle current densities, total current density in the GDG can be defined as

$$\mathbf{J}_g = e(\mathbf{\Gamma}_i - \mathbf{\Gamma}_e) = e(\mu_i n_i + \mu_e n_e)\mathbf{E} + D_e \nabla n_e - D_i \nabla n_i. \tag{2.16}$$

Lastly, the equation of thermal conductivity is defined as

$$N c_{p1} \frac{\partial T}{\partial t} + \nabla(-\lambda \nabla T) = \mathbf{J}_g \cdot \mathbf{E}. \tag{2.17}$$

c_{p1} is the heat capacity, k is the Boltzmann constant and λ is the thermal conductivity.

The system is defined by equations (2.11), (2.12), (2.13), (2.15) and (2.17). Terms that are used in these equations are shown in equations (2.8)-(2.10).

$$\begin{aligned}
\frac{\partial n_e}{\partial t} + \nabla \cdot (-\mu_e n_e \mathbf{E} - D_e \nabla n_e) &= |-\mu_e n_e \mathbf{E} - D_e \nabla n_e| \, \bar{\alpha}(|\mathbf{E}|), && (2.18)\\
\frac{\partial n_i}{\partial t} + \nabla \cdot (\mu_i n_i \mathbf{E} - D_i \nabla n_i) &= |-\mu_e n_e \mathbf{E} - D_e \nabla n_e| \, \bar{\alpha}(|\mathbf{E}|), && (2.19)\\
\nabla \cdot \mathbf{E} &= \frac{e}{\epsilon_0}(n_i - n_e), \quad 0 \le y \le d_g && (2.20)\\
\nabla \cdot \mathbf{E} &= 0, \qquad d_g \le y \le d_g + d_s && (2.21)\\
N c_{p1} \frac{\partial T}{\partial t} + \nabla(-\lambda \nabla T) &= \mathbf{J}_g \cdot \mathbf{E}. && (2.22)
\end{aligned}$$

Within the 1D model, equations of the system are solved along normal to the electrodes.

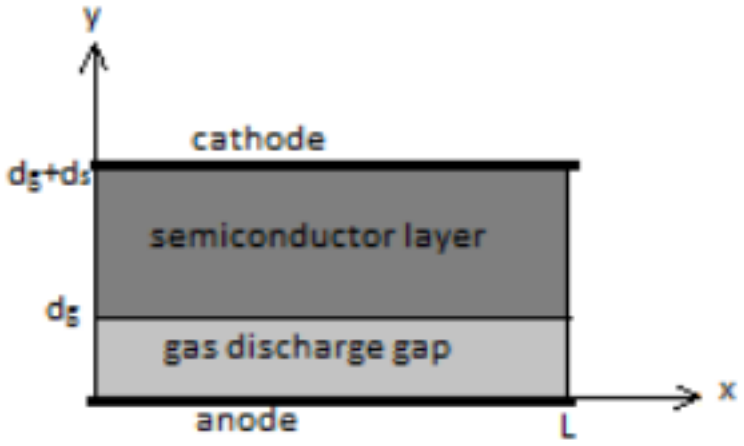

Figure 2.2: Boundary conditions on the 2D model.

2.2 Boundary Conditions

The system is schematically shown in figure 2.2. Thickness of the GDG region is d_g and it is d_s for SC region. The anode is at $y = 0$ and the cathode is at $y = d_g$. At the anode, ion current flux is zero,

$$\mathbf{\Gamma_i}(x, 0, t) = 0. \tag{2.23}$$

If the diffusion flux is neglegible, then the ion density is also zero there. Thus, the boundary condition at $y = 0$

$$n_i(x, 0, t) = 0. \tag{2.24}$$

Remaining conditions at anode, $y = 0$, are given below

$$\begin{aligned} n_e \frac{\bar{v_e}}{4} - \frac{1}{2}(-n_e \mu_e \mathbf{E} - D_e \nabla n_e) &= 0, & (2.25)\\ \varphi_g &= U_t, & (2.26)\\ \frac{\partial T}{\partial y} &= 0, & (2.27) \end{aligned}$$

where U_t is the applied voltage and $\bar{v_e} = (8kT_e/(\pi m_e))^{1/2}$ is the electron thermal velocity [7].

Secondary electron emission (γ-process) occurs at cathode. For this condition diffusion term can be neglegible since it is too small. In this case, the boundary condition at $y = d_g$ is related with the γ-process which is defined as electron emission process by ions,

$$|\mathbf{\Gamma}_e(x, d_g, t)| = \gamma \, |\mathbf{\Gamma}_i(x, d_g, t)| \,, \tag{2.28}$$

from which

$$\mu_e n_e(x, d_g, t) = \gamma \mu_i n_i(x, d_g, t). \tag{2.29}$$

Electric potentials for GDG and SC are taken equal to each other at $y = d_g$ because electric potential is continuous,

$$\varphi_g(x, d_g, t) = \varphi_s(x, d_g, t). \tag{2.30}$$

However, current density of GDG is different from SC's and hence electric field values are different at $x = d_g$. In this case, they become equal using Maxwell-Ampere law

$$\mathbf{J}_g + \epsilon_0 \partial_t \mathbf{E} = \mathbf{J}_s + \epsilon_0 \partial_t \mathbf{E}, \tag{2.31}$$

It is useful to rewrite in the following form:

$$\partial_t \Sigma = (\mathbf{J}_g - \mathbf{J}_s) \cdot \mathbf{n}, \tag{2.32}$$

where Σ is the surface charge density defined at $y = d_g$ by

$$\Sigma = (\epsilon\epsilon_0 \mathbf{E}_s - \epsilon_0 \mathbf{E}_g) \cdot \mathbf{n}. \tag{2.33}$$

Remaining conditions at cathode, $y = d_g$,

$$\frac{\partial n_i}{\partial y} = 0 \tag{2.34}$$

$$T = T_0. \tag{2.35}$$

Finally, at $y = d_g + d_s$, electric potantial is $\varphi_s = 0$.

At the lateral boundaries, $x = 0$ and $x = l$, we impose homogeneous Neumann

$$\frac{\partial n_e}{\partial x} = 0, \tag{2.36}$$

$$\frac{\partial n_i}{\partial x} = 0, \tag{2.37}$$

$$\frac{\partial \varphi_g}{\partial x} = 0, \tag{2.38}$$

$$\frac{\partial \varphi_s}{\partial x} = 0, \tag{2.39}$$

$$\frac{\partial T}{\partial x} = 0. \tag{2.40}$$

2.2.1 Boundary Conditions for 1D

Boundary conditions for 1D case are the same conditions as given above but restricted by y-direction. At the anode $y = 0$,

$$n_i(0, t) = 0 \tag{2.41}$$

$$n_e \frac{\bar{v_e}}{4} - \frac{1}{2}(-n_e \mu_e \mathbf{E} - D_e \nabla n_e) = 0, \tag{2.42}$$

$$\varphi_g(0, t) = U_t \tag{2.43}$$

$$\frac{\partial T}{\partial x} = 0. \tag{2.44}$$

At the boundary point between GDG and SC,

$$\begin{aligned} \partial_t \Sigma &= (\mathbf{J}_g - \mathbf{J}_s) \cdot \mathbf{n}, && (2.45) \\ \Sigma &= (\epsilon\epsilon_0 \mathbf{E}_s - \epsilon_0 \mathbf{E}_g) \cdot \mathbf{n}, && (2.46) \\ \varphi_s(d_g, t) &= \varphi_g(d_g, t), && (2.47) \\ n_e(d_g, t) &= \gamma\mu n_i(d_g, t). && (2.48) \end{aligned}$$

At $y = d_g + d_s$,

$$\varphi_s(d_g + d_s, t) = 0. \quad (2.49)$$

2.3 Dimensional Analysis

Equations that represents the system include variables and parameters. Variables are two types namely dependent and independent. Dependents are obtained after getting solution of the equations. They are unknowns and they are solved at different conditions. Thus, they depend on the other variables. Independent variables are exactly what it sound like. They do not change by other variables. In this case for example, density of the particles are dependent variables and they depend on time and position but time and position are independent variables [19].

Units, or dimensions, describe the parameters or variables as categorizing them. They give an idea about its physical properties. In Table 2.1, some dimensions that are used in this work is given,

Table2.1: Some dimensions used in this work.

symbol	dimension	unit
d	length	cm
t	time	s
T	temperature	K
p	pressure	Torr
σ	conductivity	$\Omega^{-1}\text{cm}^{-1}$
μ	mobility	$\text{cm}^2\text{V}^{-1}\text{s}^{-1}$
D	diffusion coefficient	cm^2s^{-1}
U	voltage	V
n	particle density	cm^{-3}
J	current density	μ A cm^{-2}

Although dimensions are necessary to understand the physical property of the system, reduction of the equations to the dimensionless form have some advantages to solve them. Making this reduction, total number of variables and parameters are reduced to the minimal. Another advantage is that equations become less complex case and then analysis of them is simplifier. Finally, when the model is nondimensionalized properly, more important and less important

terms (and process) can be distinguished by comparison with unity.

In this section, dimensional analysis of equations (2.22) are explained. Thus, it is important to define new parameters. New dimensionless parameters and variables are $\alpha_0 = Ap$, $E_0 = Bp$, $\tau = t/t_0$, $t_0 = (\alpha_0 \mu_e E_0)^{-1}$, $\mathcal{E} = \mathbf{E}/E_0$, $\rho = n_i/n_0$, $\mu = \mu_i/\mu_e$, $X = x/X_0$, $X_0 = \alpha_0^{-1}$, $\sigma = n_e/n_0$, $q_0 = \epsilon_0 \alpha_0 E_0$ and $n_0 = q_0/e$.

Equations with these parameters are called as dimensionless group [20]. Then, inserting these parameters such as n_e, t, x and E into continuity equation for electron, we obtain

$$\frac{n_0}{t_0}\frac{\partial \sigma}{\partial \tau} + \frac{1}{X_0}\frac{\partial}{\partial X}(-\mu_e n_0 \sigma \mathcal{E} E_0 - \mu_e T_e \frac{n_0}{X_0}\frac{\partial \sigma}{\partial X}) = n_0 \mu_e E_0 |-\sigma\mathcal{E} - D_e \frac{\partial \sigma}{\partial X}|\alpha_0 e^{-\frac{E_0}{\mathcal{E}E_0}}. \tag{2.50}$$

It is the equality $D_e = \mu_e T_e$ in this equation. Then, multiplying each term with t_0/n_0 and using definition of the terms t_0 and X_0 it yields

$$\frac{\partial \sigma}{\partial \tau} + \frac{\partial}{\partial X}(-\mathcal{E}_g \sigma - D_e \frac{\partial \sigma}{\partial X}) = |-\mathcal{E}\sigma - D_e \frac{\partial \sigma}{\partial X}|e^{-\frac{1}{\mathcal{E}}}. \tag{2.51}$$

Similarly, it can done for ions continuity equation. In this equation, it is used $D_i = \mu_i T_i$ for diffusion term

$$\frac{\partial \rho}{\partial \tau} + \frac{\partial}{\partial X}(\mu\mathcal{E}\rho - \mu D_i \frac{\partial \rho}{\partial X}) = |-\mathcal{E}\sigma - D_e \frac{\partial \sigma}{\partial X}|e^{-\frac{1}{\mathcal{E}}}. \tag{2.52}$$

Using $\mathcal{E}$, X, n_i and n_e we obtain dimensionless Poisson equation,

$$\frac{E_0}{X_0}\frac{\partial \mathcal{E}}{\partial X} = \frac{e}{\epsilon_0}(\rho - \sigma)n_0, \tag{2.53}$$

from which

$$\frac{\partial \mathcal{E}}{\partial X} = \rho - \sigma, \quad \mathcal{E} = -\frac{\partial \varphi_g}{\partial X}. \tag{2.54}$$

Equation for SC region is written as

$$\frac{E_0}{X_0}\frac{\partial \mathcal{E}}{\partial X} = 0, \quad \mathcal{E} = -\frac{\partial \varphi_s}{\partial X}, \tag{2.55}$$

from which

$$\frac{\partial \mathcal{E}}{\partial X} = 0. \tag{2.56}$$

Electric potential is continuous. This means that, it can be calculated in GDG region and in SC region. To get the dimensionless version of it, parameters t_0, μ_i, n_i and E are substituted into equation (2.32) to have

$$\frac{1}{t_0}\frac{\partial \Sigma}{\partial \tau} = e(1+\gamma)\mu\mu_e n_0 \rho E_0 \mathcal{E} + e\mu_e D_e \frac{\partial \sigma}{\partial X} - e\mu\mu_e D_i \frac{\partial \rho}{\partial X} - \sigma_s \mu_e q_0 E_0 \mathcal{E}. \tag{2.57}$$

Using the definition $\sigma_s = \bar{\sigma_s}/(\mu_e q_0)$ and multiplying with $t_0\alpha_0/q_0$. We get the dimensionless version of the surface charge density. It is $Q = \Sigma\alpha_0/q_0$. Then,

$$\frac{\partial Q}{\partial \tau} = [(1+\gamma)\mu\rho\mathcal{E} + D_e \frac{\partial \sigma}{\partial X} - \mu D_i - \sigma_s \mathcal{E}]. \tag{2.58}$$

Before getting the case for thermal conductivity equation, the heat diffusion coefficient must be defined. It is also known as thermometric conductivity and it is $\chi = \lambda/(n_0 c_{p1})$ where λ is the thermal conductivity constant.[21]. When the equation is multiplied with $t_0\alpha_0^2$, it becomes dimensionless:

$$\frac{n_0 c_{p1}}{t_0}\frac{\partial T}{\partial t} + \frac{1}{X_0}\frac{\partial}{\partial X}\left(-\frac{\lambda}{X_0}\frac{\partial T}{\partial X}\right) = \mathcal{E}\frac{E_0^2 e n_0 \mu_e}{E_0 X_0}\left(\rho\mu\mathcal{E} + \sigma\mathcal{E} + T_e\frac{\partial\sigma}{\partial X} - \mu T\frac{\partial\rho}{\partial X}\right). \tag{2.59}$$

$\zeta = (t_0\alpha_0^2\lambda)/(n_0 c_{p1})$ is dimensionless constant. When each term is multiplied with $(t_0)/(n_0 c_{p1})$ and t_0 parameter is written in the equation, then it is obtained in the final form

$$\frac{\partial T}{\partial \tau} + \zeta\frac{\partial^2 T}{\partial X^2} = \mathcal{E}\left(\rho\mu\mathcal{E} + \sigma\mathcal{E} + D_e\frac{\partial\sigma}{\partial X} - D_i\frac{\partial\rho}{\partial X}\right). \tag{2.60}$$

The complete system of equations in dimensionless form becomes

$$\begin{aligned}
\frac{\partial\sigma}{\partial\tau} + \frac{\partial}{\partial X}(-\mathcal{E}_g\sigma - D_e\frac{\partial\sigma}{\partial X}) &= |-\mathcal{E}\sigma - D_e\frac{\partial\sigma}{\partial X}|e^{-\frac{1}{\varepsilon}}, && (2.61)\\
\frac{\partial\rho}{\partial\tau} + \frac{\partial}{\partial X}(\mu\mathcal{E}\rho - \mu D_i\frac{\partial\rho}{\partial X}) &= |-\mathcal{E}\sigma - D_e\frac{\partial\sigma}{\partial X}|e^{-\frac{1}{\varepsilon}}, && (2.62)\\
\frac{\partial\mathcal{E}}{\partial X} &= \rho - \sigma, \quad 0 \le y \le d_g && (2.63)\\
\frac{\partial\mathcal{E}}{\partial X} &= 0, \qquad d_g \le y \le d_g + d_s && (2.64)\\
\frac{\partial T}{\partial\tau} + \zeta\frac{\partial^2 T}{\partial X^2} &= \mathcal{E}\cdot\left(\rho\mu\mathcal{E} + \sigma\mathcal{E} + D_e\frac{\partial\sigma}{\partial X} - D_i\frac{\partial\rho}{\partial X}\right). && (2.65)
\end{aligned}$$

2.4 Adiabatic Elimination of Electrons

Adiabatic elimination is a useful method that allows to enhance the computational efficiency [22]. It is based on that calculations are done using the time scale. In this case, the fast variable dynamics can be eliminated choosing slow variables properties in calculations, which reach the solution over large time scale. When the slow varibles reach the solution, fast variables has already been in equilibrium.

In this system, electrons are more mobile and lighter compearing to ions. Then, the time parameter changes to $t_0^i = 1/(\alpha_0\mu_i E_0)$ [17]. Conductivity of the semiconductor also becomes dimensionless multiplying by $1/(\mu_i q_0)$. Using these

changed parameters, system equations are

$$\frac{\partial}{\partial x}\left(-s\mathcal{E}-D_e\frac{\partial s}{\partial X}\right) = exp\left(-\frac{1}{\mathcal{E}}\right)\left|-s\mathcal{E}-D_e\frac{\partial s}{\partial X}\right| \quad (2.66)$$

$$\frac{\partial \rho}{\partial \tau_i}+\frac{\partial}{\partial X}\left(\rho\mathcal{E}-D_i\frac{\partial \rho}{\partial X}\right) = exp\left(-\frac{1}{\mathcal{E}}\right)\left|-s\mathcal{E}-D_e\frac{\partial s}{\partial X}\right| \quad (2.67)$$

$$\frac{\partial \mathcal{E}}{\partial x} = \rho, \quad (2.68)$$

$$\frac{\partial T}{\partial \tau_i}+\frac{\zeta}{\mu}\frac{\partial^2 T}{\partial X^2} = \mathcal{E}\left(\rho\mathcal{E}+s\mathcal{E}+D_e\frac{\partial \sigma}{\partial X}-D_i\frac{\partial \rho}{\partial X}\right). \quad (2.69)$$

In equations, electron density is calculated as $s=\sigma/\mu$ in the limit as $\mu \to 0$. In this case, continuity equation for electron turns into stationary equation. It is expected to get solutions $1/\mu$ times faster compared to the other calculations.

2.5 Parameter Regime

In this part, parameters are described. Two sets of parameters are considered. In 1D calculations, it was used the parameters given in Table 2.2 to get the Lorenz map solution, [16],

Table2.2: Parameters used to get Lorenz map, [16].

symbol	value	definition
U_t	$513-570$ V	applied voltage
p	30 Torr	pressure
d_g	0.1 cm	thickness of the GDG
d_s	0.12 cm	thickness of the SC
σ	$(2.6\times 10^5 \Omega\text{cm})^{-1}$	conductivity
μ	0.0035	mobility ratio
γ	0.08	secondary emission coefficient
ϵ_s	13.1	dielectric constant

Parameters given in table 2.3 were used in 1D and 2D calculations. They were used before in the experiment and also in the theoretical works [7, 15].

Table2.3: Parameters used to 1D and 2D solutions, [7].

symbol	value	definition
U_t	$2397 - 2473$ V	applied voltage
p	211.52 Torr	pressure
d_g	0.044 cm	thickness of the GDG
d_s	0.1 cm	thickness of the SC
σ	1.3×10^{-8} Ω^{-1}cm^{-1}	conductivity
T_e	6 eV	electron temperature
D_e	4260 cm^{2}s^{-1}	diffusion coefficient for e^-
D_i	0.016 cm^{2}s^{-1}	diffusion coefficient for ions
μ	0.0026	mobility ratio
γ	0.0026	secondary emission coefficent
ϵ_s	11.7	dielectric constant
A	12 cm^{-1}Torr^{-1}	constant for Townsend coefficent
B	342 V cm^{-1}Torr^{-1}	constant for Townsend coefficent
χ	0.22555 m^{2}s^{-1}	thermal diffusion coefficent

2.6 Scharfetter Gummel Method

Scharfetter Gummel is used to solve drift-diffusion equations. It is assumed that current density is constant [23]. Thus,

$$\frac{d\Gamma_e}{dx} = 0. \tag{2.70}$$

Using definition of the current density in equation-5, it can be obtained the derivative of the electron density as

$$\frac{\partial \sigma}{\partial x} = -\frac{\sigma \mu_e E}{D}_e - \frac{\Gamma_e}{D_e}. \tag{2.71}$$

It is defined the term as $u = \sigma + \Gamma_i/(\mu_e E)$ for simplicity,

$$\frac{\partial u}{\partial x} = \frac{\partial \sigma}{\partial x} \tag{2.72}$$

$$= -\left(\sigma + \frac{\Gamma_i}{\mu_e E}\right)\frac{\mu_e E}{D_e} \tag{2.73}$$

$$= -u\frac{\mu_e E}{D_e}. \tag{2.74}$$

Then, the solution of u is $u = Cexp(-\mu_e E h/D_e)$. In here, C is a constant and h is the interval between two points. To get rid of C the ratio of values of u at

point i and $i+1$,

$$\frac{u_{i+1}}{u_i} = \frac{Cexp(-\frac{\mu_e E(i+1)h}{D_e})}{Cexp(-\frac{\mu_e E(i)h}{D_e})} \tag{2.75}$$

$$= Cexp(-\frac{\mu_e Eh}{D_e}) \tag{2.76}$$

$$= \frac{\sigma_{i+1} + \frac{\Gamma_{i+1/2}}{\mu_e E}}{\sigma_i + \frac{\Gamma_{i+1/2}}{\mu_e E}}. \tag{2.77}$$

The current density is calculate at $i+1$. Using above equality,

$$\Gamma ii + 1/2 = -\frac{\mu_e E}{1 - exp(-\frac{\mu_e Eh}{D_e})}\sigma_i - \frac{\mu_e E}{1 - exp(-\frac{\mu_e Eh}{D_e})}\sigma_{i+1} \tag{2.78}$$

$$= \alpha_e \sigma_i - \beta_e \sigma_{i+1}. \tag{2.79}$$

is obtained. Lastly, the continuity equation must be expressed in implicit form.

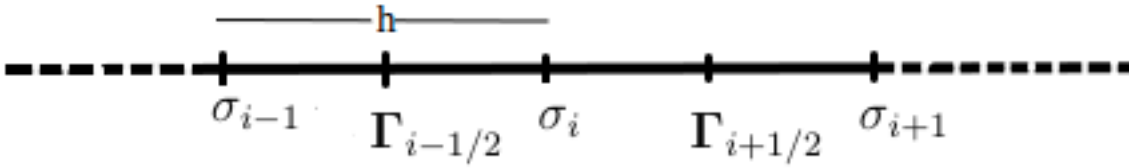

Figure 2.3: Current flux in 1D.

In figure-2.3, it is seen that the interval d_g is divided into N equal part as length h. Similarly, time is also divided into small pieces as τ that is used as time step. $n+1$ refers to calculations at that time and n belongs to previous calculations.

$$\frac{\partial \sigma}{\partial t} = \frac{\sigma_i^{n+1} - \sigma_i^n}{\tau}, \tag{2.80}$$

$$\frac{\partial \Gamma}{\partial x} = \frac{\Gamma_{i+1/2} - \Gamma_{i-1/2}}{h} \tag{2.81}$$

$$= -\frac{\alpha_e \sigma_{i-1} + (\alpha_e + \beta_e)\sigma_i - \beta_e \sigma_{i+1}}{h}. \tag{2.82}$$

The final version of the continuity equation for electrons is given below,

$$-\left(\frac{\tau\alpha}{h}\right)\sigma_{i-1}^{n+1} + \left(1 + \frac{(\alpha+\beta)\tau}{h}\right)\sigma_i^n - \left(\frac{\tau\beta}{h}\right)\sigma_{i+1}^{n+1} = \tag{2.83}$$

$$\sigma_i^n + \tau\alpha_0 exp\left(\frac{-E_0}{E_i^n}\right)|\alpha^n\sigma_i^n - \beta^n\sigma_i^n|. \tag{2.84}$$

Similarly, for ions

$$-\left(\frac{\tau\alpha_i}{h}\right)\rho_{i-1}^{n+1} + \left(1 + \frac{(\alpha_i+\beta_i)\tau}{h}\right)\rho_i^n - \left(\frac{\tau\beta_i}{h}\right)\rho_{i+1}^{n+1} = \tag{2.85}$$

$$\sigma_i^n + \tau\alpha_0 exp\left(\frac{-E_0}{E_i^n}\right)|\alpha_e^n\sigma_i^n - \beta_e^n\sigma_i^n|. \tag{2.86}$$

Exponential values for ions are

$$\alpha_i = \frac{\mu_i E_i}{1 - exp(\frac{-\mu_i E_i h}{D_i})}, \quad \beta_i = -\frac{\mu_i E_i}{1 - exp(\frac{\mu_i E_i h}{D_i})}. \tag{2.87}$$

Implicit forms for equation that are used to solve electric potentials at GDG and SC

$$-\varphi_{i-1} + 2\varphi_i - \varphi_{i+1} = \frac{eh}{\epsilon_0}(\rho_i - \sigma_i) \ , \ [0, d_g] \tag{2.88}$$

$$-\varphi_{i-1} + 2\varphi_i - \varphi_{i+1} = 0 \qquad , \ [d_g, d_s] \tag{2.89}$$

For the boundary between GDG and SC regions, given at the below equation is used,

$$J_g + \epsilon_0 \frac{E}{\partial t} = J_s + \epsilon\epsilon_0 \frac{E_s}{\partial t} \tag{2.90}$$

Then, this equation is explained detailly at boundary conditions part.

$$\frac{\partial}{\partial t}(-\epsilon_0 E + \epsilon\epsilon_0 E_s) = J_g - J_s \tag{2.91}$$

$$\frac{\partial Q_{surf}}{\partial t} = J_g - J_s \tag{2.92}$$

$$= (\rho\mu_i E + \sigma\mu_e E + D_e \frac{\partial\sigma}{\partial t} - D_e \frac{\partial\rho}{\partial t}) - \sigma_s E_s. \tag{2.93}$$

2.7 Boundary Conditions for Scharfetter Gummel Method

At anode $\varphi = 0$, surface charge density is used as flux term,

$$-\epsilon_0 \frac{\partial\varphi}{\partial x} = \epsilon_0 \frac{\varphi}{d_g} - Q_{surf} \tag{2.94}$$

$$-\epsilon_0 \frac{\varphi_N - \varphi_{N-1}}{h} = \epsilon_0 \frac{\varphi_N}{d_g} - Q_{surf}. \tag{2.95}$$

Then, the equation used at that boundary is

$$-\left(\frac{\epsilon_0}{h}\right)\varphi_{N-1} + \epsilon_0 \left(\frac{1}{L} + \frac{1}{h}\right)\varphi_N = Q_{surf}. \tag{2.96}$$

Then, conditions are $\varphi_s(d_g) = \varphi_N$ and $\varphi_s(d_g + d_s) = -U_t$ where U_t is applied voltage. Boundary conditions for electron density

$$\sigma_2 - \sigma_1 = 0, \tag{2.97}$$

$$\sigma_N = \gamma\mu\rho_N \tag{2.98}$$

For ions density

$$\rho_1 = 0 \tag{2.99}$$

$$\rho_N - \rho_{N-1} = 0. \tag{2.100}$$

CHAPTER 3

NUMERICAL RESULTS

3.1 1D Analysis

Results are obtained using COMSOL® version 4.3 and MATLAB®. Equations that are used in the model are explained in previous chapter. 1D and 2D solutions are obtained in COMSOL® solving dimensionless form of the equations. In 1D, equations were solved after adiabatic elimination of electrons. In this case, the aim is to get the solutions in shorter time. Using MATLAB®, equation are resolved using Scharfetter Gummel method. In this part, these solutions are compared with each other and with the literature.

To get the Lorenz map, it was used 1D mesh with number of grid 200. The time step was 2.03×10^{-10} s and calculations were performed until 2.44×10^{-4} s.

All 1D calculations were perfomed on a 120 spatial grid for GDG region and

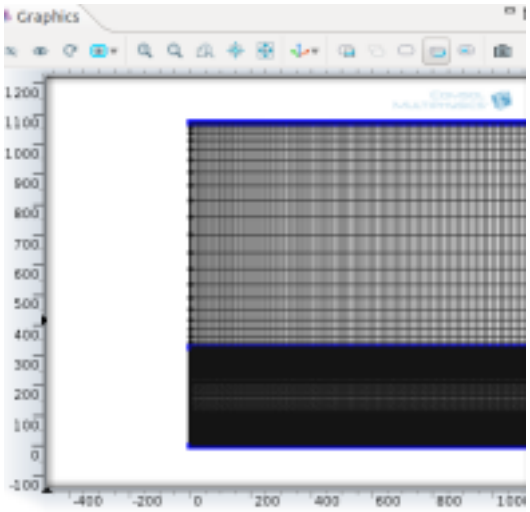

Figure 3.1: 2D mesh in Comsol®.

on 50 spatail grid for SC region. Maximum time step was 1.33×10^{-4} s. Implicit backward differential formulas (BDF) was chosen as a time step solver method. By this method, COMSOL® kept the solution of the previous step and it used them to get the next one. In this case, time step was not constant. It changes

during the calculation because it tries to get smaller error than absolute tolerance defined in the solver. In this case, the spatial grid was 120×800 spatial grid for GDG region and 50×800 for SC region as shown in figure 3.1. Mesh points were distributed symmetrically along the boundaries. It was assumed that patterns appear due to the nonlinearity of the gas discharge. In this case, semiconductor is a weakly conducting material. Thus, it was chosen that SC grid number is less than GDG's [7].

In COMSOL®, continuity equations and heat equation were added the model in *Transport of Diluted Species* form. Electric potentials for each region were calculated by *Poisson equation* form. *Weak form boundary PDE* form was used to get the solution of the surface charge.

The grid point number was the same with the 1D COMSOL® for Scharfetter Gummel method. This method was performed on MATLAB®. Time step was 10^{-15} s and it was not constant. The control parameter is ratio of the minimum value of the electric field value to the current density. The end time was 8.94×10^{-4} s. It was enough to get the acceptable solution.

In these calculations, two different regimes are investigated. The main difference between them applied voltage as $U_t = 2473$ V and $U_t = 2397$ V. Calculated breakdown voltage by equation (1.9) is $V_t = 2327.9$ V. Characteristic value of the currents are 3.17mAcm^{-2} and 1.91mAcm^{-2} respectively by equation 1.10.

In 2D calculations, applied voltage was $U_t = 2397$ V. It was enough that calculations were perfomed only this voltage value to show patterns.

3.2 Lorenz Map

Parameters given in Table 2.2 were used in this part. These data were obtained before [16]. It was repeated to be sure the validity of the used model. In Figure 3.2, current and voltage graphs are shown. Applied voltage values are 543.11 V and 563.78 V. Oscillation results were obtained.

In Figure 3.3, current-voltage graphs were obtained changing the applied voltage slightly. Here, 534.11 V and $U_t = 548.94$ V are the critical values. Thus, current and voltage vs time graphs were plotted to compare them in figure 3.2. Number of peaks increse in the same interval as increasing applied voltage in that figure. This interval is the one period of the solution. If it is excepted the first solution in *(a)* figure 3.3, it becomes double in *(b)*. It is called period doubling cascade [20]. Each graph was plotted in the same interval. Increasing the applied voltage, it repeats itself and the system translate to the chaotic regime.

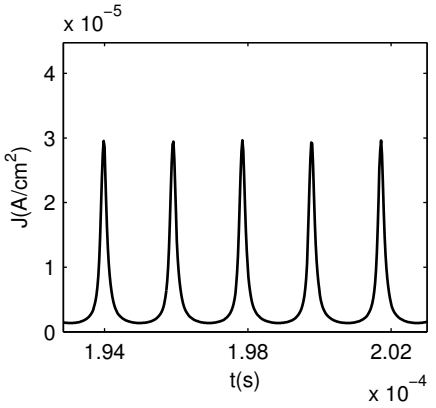

(a)

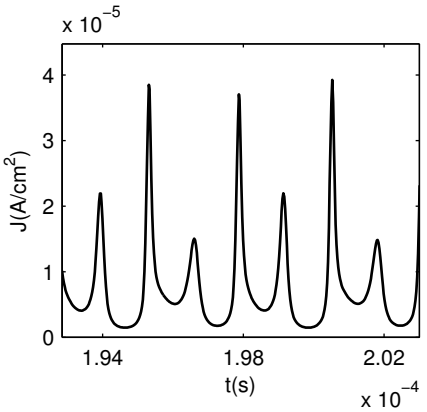

(b)

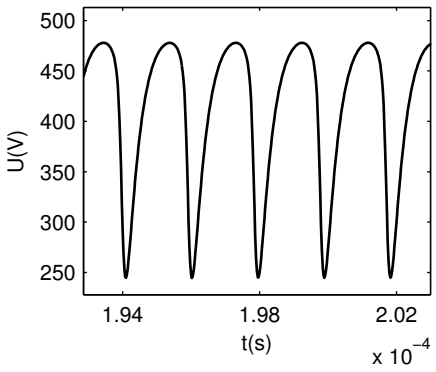

(c)

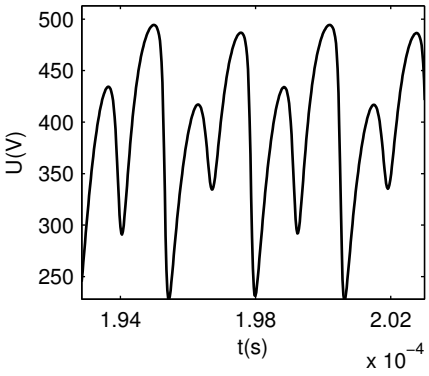

(d)

Figure 3.2: Current and voltage vs time graphs, applied voltage (a) and (c) $U_t = 534.11$ V, (b) and (d) $U_t = 563.78$ V, conditions are given in Table 2.2.

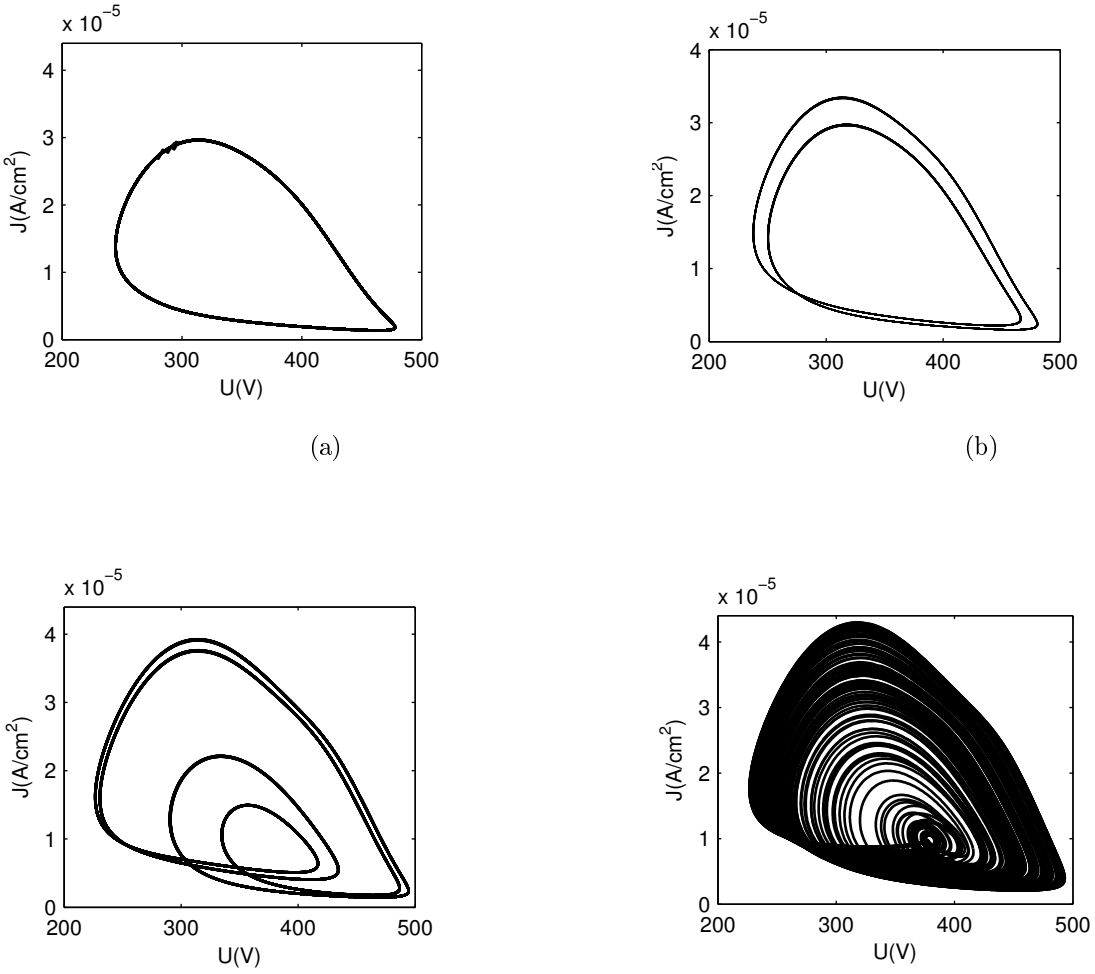

(a) (b)

(c) (d)

Figure 3.3: Phase portraits of orbits, current vs voltage, applied voltage U_t (a) 534.11 V, (b) 548.94 V, (c) 563.78 V, (d) 593.45 V, remaining conditions are as in Figure 3.2.

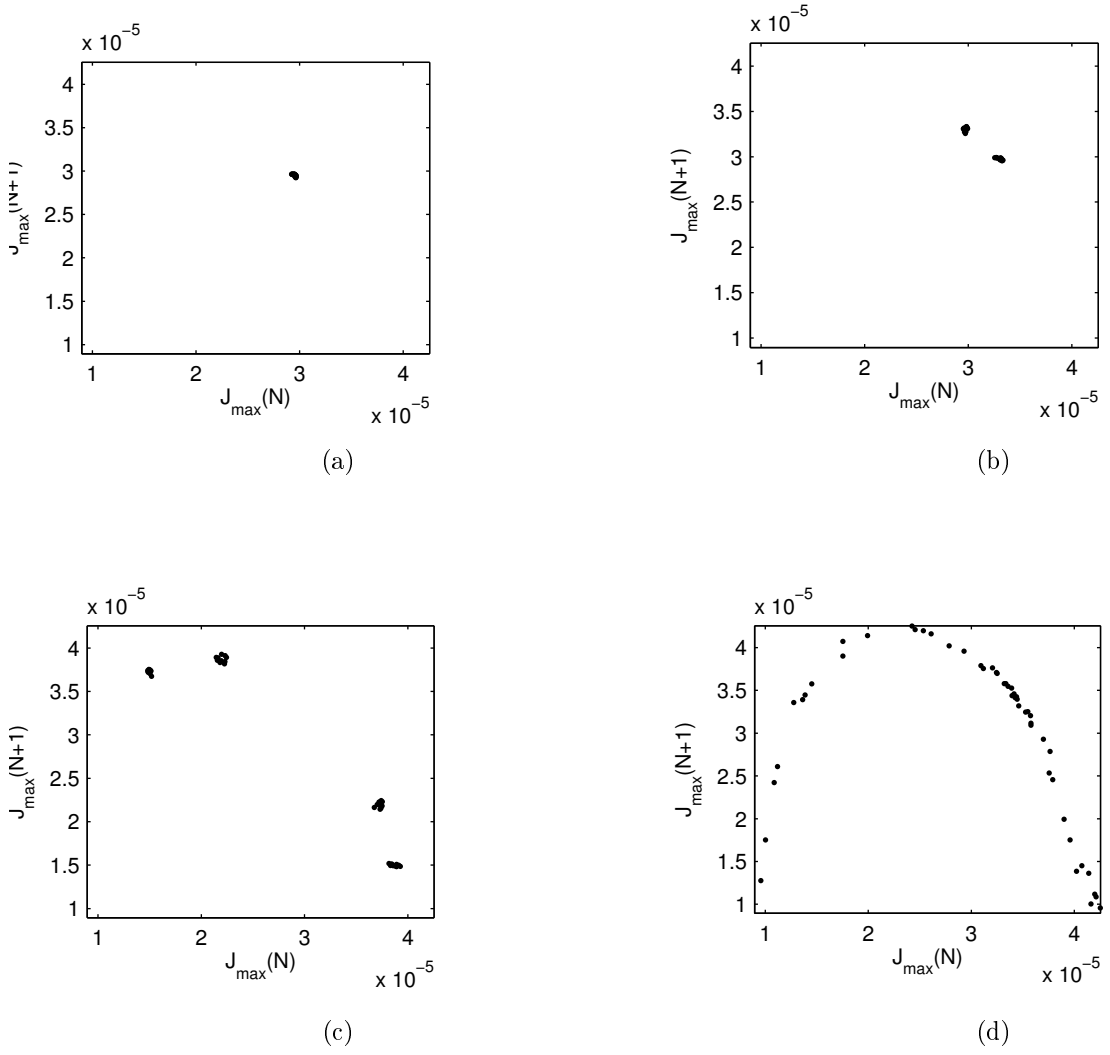

Figure 3.4: Lorenz map, applied voltage U_t(a) 534.11 V, (b) 548.94 V, (c) 563.78 V, (d) 593.45 V remaining conditions are as in Figure 3.2.

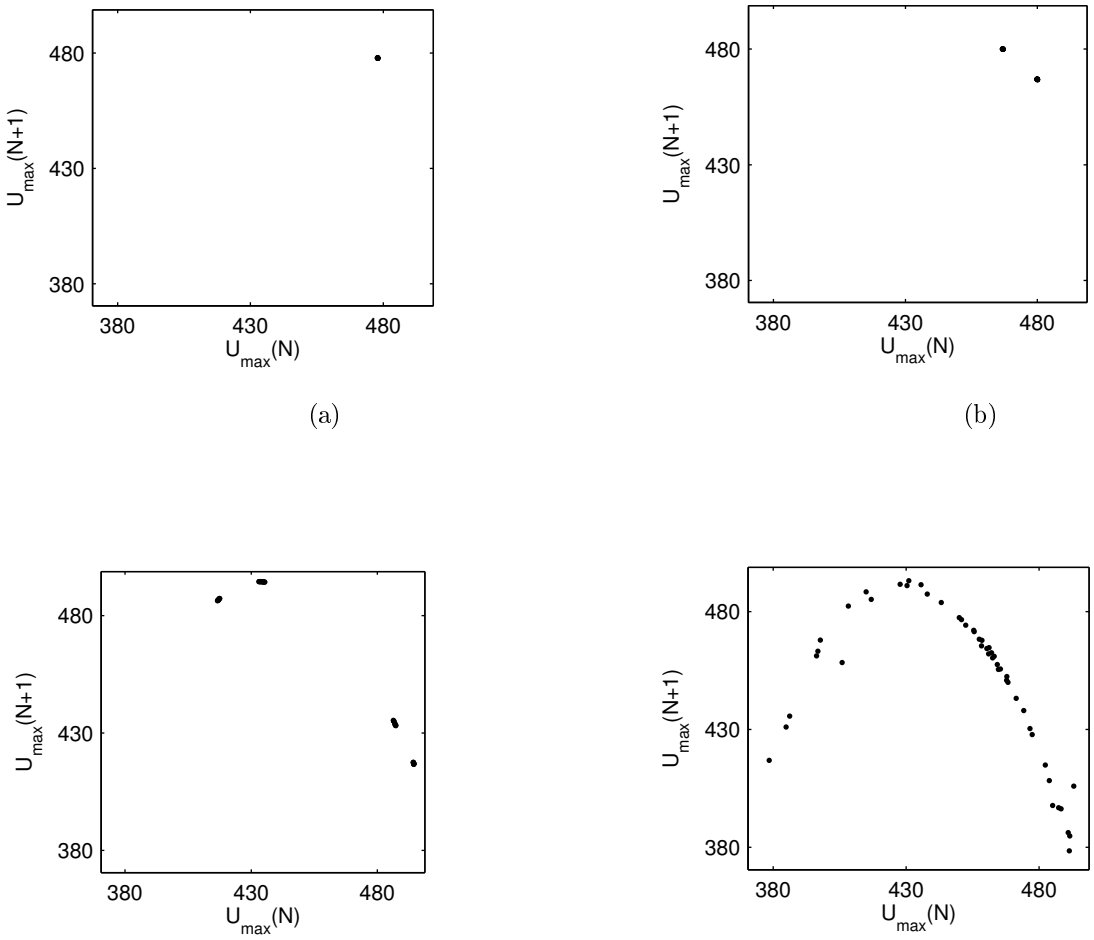

(a) (b)

(c) (d)

Figure 3.5: Lorenz map, applied voltage U_t (a) 534.11 V, (b) 548.94 V, (c) 563.78 V, (d)593.45 V, remaining conditions are as in figure 3.2.

Then, it is necessary to show that the system goes to the chaotic phase in different way. It is to get the Lorenz map of the solutions at the critical values.

Edward Norton Lorenz, the pioneer of the chaos theory, said that (1963) :

the trajectory appearently leaves one spiral only after exceeding some critical distance from the center. Moreover, the extend to which this distance is exceeded appears to determine the point at which the next spiral is centered; this in turn seems to determine the number of circuits to be executed before changing spirals again. It therefore seems that some single feature of a given circuit should predict the same feature of the following circuit

This means that the following peak value in the oscillating system can be predicted by the previous one. Number of the local maxima gives an idea about the period of the system. This means that maxima points increases as the control parameter increases [20]. Thus, the Lorenz map of the current and voltage values are plotted because of the oscillating character of them. In Figure 3.4 and 3.5, they are shown.

It can be obviously seen that number of peaks are increasing and graph becomes of unimodal shape as increasing the applied voltage. Then, the transformation to the chatic behavior can be seen in Figure 3.3.

Differently, Lorenz map of the oscillating solutions were obtained in this work. These oscillations are periodic for both voltage and current data. Thus, parabolic character can be seen obviously in each Figure 3.5 and 3.4. Then, it can be said that the system behaves chaotically as applied voltage increses.

3.3 Effect of the Modeling Approaches

The results are shown in Figure 3.6. There, three different solutions are plotted. The first solution which is shown in blue is the solution of the total system. It is the 1^{st} case. In calculations, all system equations that are explained in previous chapter were used to solve it. The second solution in red does not include the heat equation in calculation. It is the 2^{nd} case. The temperature of the gas is constant at 100 K. The effect of this equation in the solutions is compared as taken the temperature value constant. The third solution, 3^{rd} case, in green does not include the diffusion term. It is neglected for this case and its effect is observed.

In the Figure 3.6, whole solutions give nearly the same results. Current and voltage values go to stationary solution after damping oscillation. Voltage values converge to the breakdown voltage. This is consistent with the experimental results [15]. Current values are also consistent but they are far from the characteristic value of it. Experimental conditions provide this low current values. It was done in cryogenic condition and in the high pressure. Characteristics of the

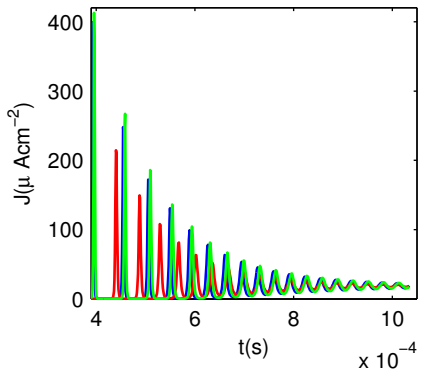

(a)

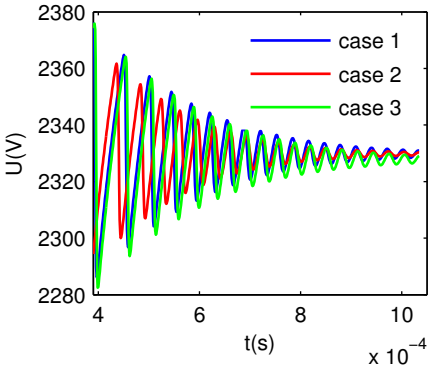

(b)

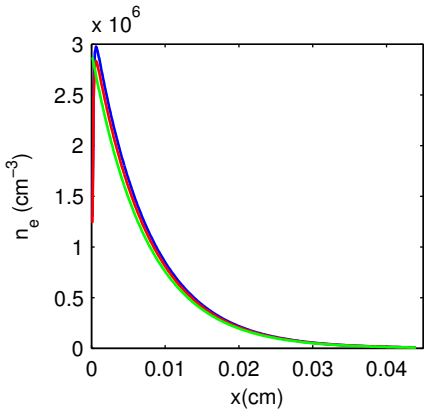

(c)

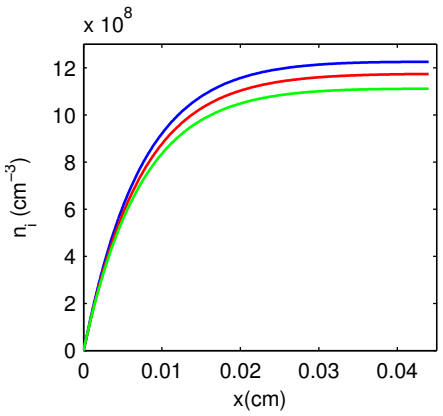

(d)

Figure 3.6: 1d solutions along normal to the electrodes on GDG, (case 1)temperature effect, (case 2)constant temperature, (case 3) negligible diffusion (a)voltage on the GDG-SC boundary, (b)current density on the GDG-SC boundary, (c)electron density, (d)ion density, applied voltage $U_t = 2473$ V.

semiconductor also cause this effect. It is assumed in the introduction chapter.

The system was solved as DBD system eliminating the heat equation. In this case, nonlinearity of the discharge is caused by the redistribution of the electric field along the current density [7]. Then, it is shown that this system can be solved as DBD system.

If the temperature of the gas is taken constant, the solution is similar with others as seen in the figure 3.6. In this case, heat equation was neglected.

Convergence and oscillation behaviour of each solution are similar. At this time solution is near the stationary case but not exactly. Thus, there are small differences between them. During the calculations, changing time step can cause them. It is seen obviously current and voltage graphs. The solution in case 2^{nd} folows other solutions a bit later. It can be seen also the amplitude of the solution in case 3^{rd} is a little bit greater than the case 1^{st} at initial times. The differences nearly disappear as the solutions go to stationary state.

The third graph shows the ion density solutions. This solution is plotted before the stationary state. Thus, there is a small difference between each case. It is obvious for case 1 and 3. This difference can be also explained using figure 3.7. In this figure, temperature value changes from 118 K to 100 K along the discharge region. On the other hand, it is constant in case 2 and there is no temperature effect on case 3. Temperature affects the ion density since the diffusion constant of the ion is proportional with the gas temperature. Thus, the difference between these cases arises due to this reason. However, it is not considered mainly since the range of the solution is nearly the same for each case.

There is nearly no difference in electron density solutions. These solutions are plotted at the same time with the ion density graphs plotted. There is no difference as in ion density graph. It can be explained as the temperature of the electrons are constant for each case. Thus, it can be say that nonlinearity of the system is explained with the gas temperature.

Using adiabatic elimination method, each case are resolved. Each case reaches the steady state solution in a less time than the previous solution. For example, it is seen that there is no oscillation at time 0.00085 s in figure 3.8 but solutions still oscillate at that time in the previous figure 3.6. Moreover, ion densities are nearly the same at the stationary time. Thus, it can be said that adiabatic elimination works in this model since desired solution is obtained consuming less time.

In Figure 3.9, case 1 is the solution of the 1D system applying voltage $U_t = 2473$ V and case 2 is the solution of the same system with adiabatic elimination of electrons. The system reaches the steady state much more before with the adiabatic elimination of electrons.

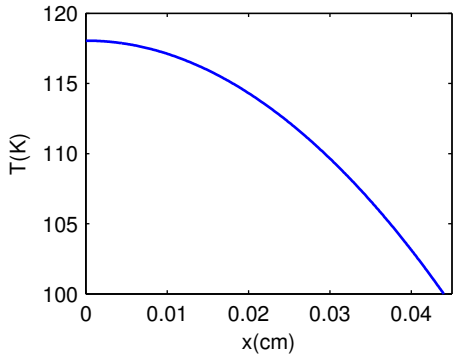

Figure 3.7: Temperature profile, conditions are same as in figure 3.6.

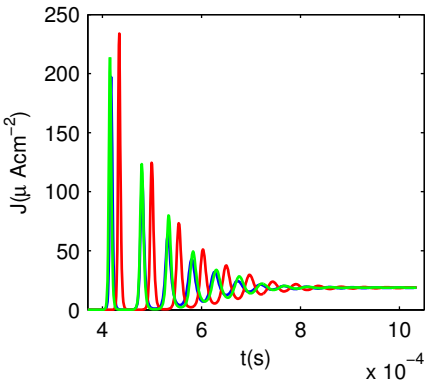

(a) current

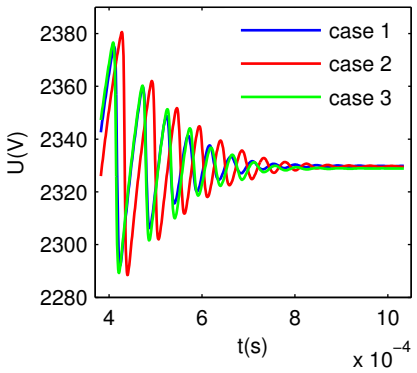

(b) electric potential

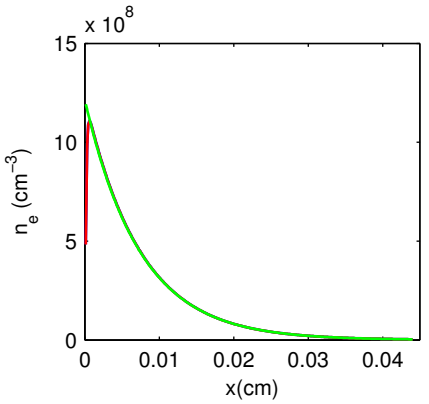

(c) electron density

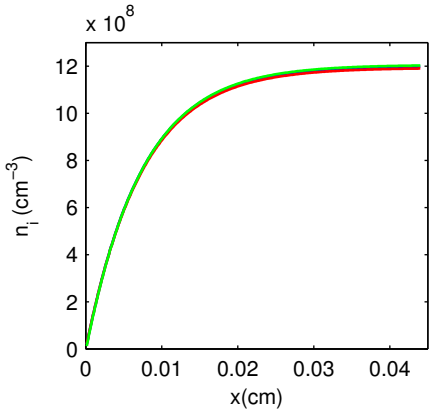

(d) ion density

Figure 3.8: 1d solutions applying adiabatic elimination, (c)current, (d)voltage, (c)ion density (d)electron density, applied voltage $U_t = 2473$ V.

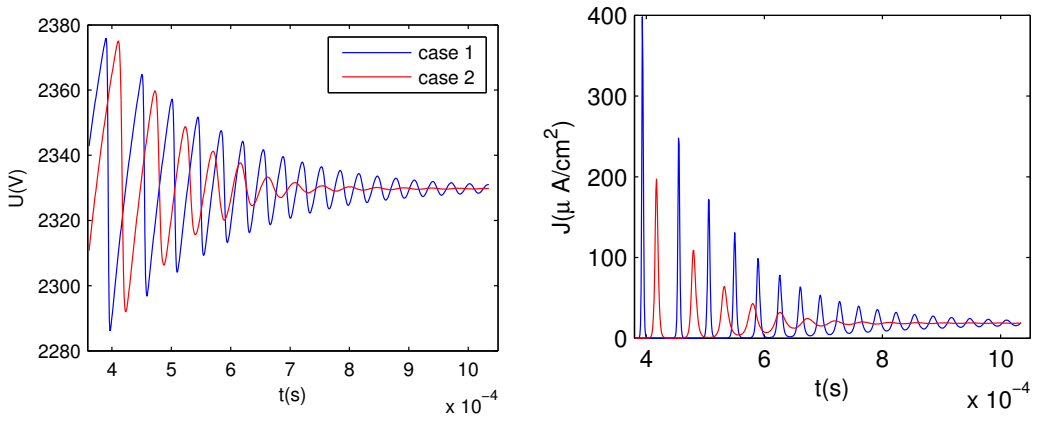

(a) (b)

Figure 3.9: Effect of the adiabatic elimination of electrons, (case1)1D solution, (case 2)1D soltion by adiabatic elimination of electrons.

3.4 Results by Scharfetter Gummel

The 3^{rd} case was solved in MATLAB® using Scharfetter Gummel method. Solutions are shown in Figure 3.10. Both solutions are converges to the breakdown voltage in the voltage graphs. Current values converges to the $J = 20.16\ \mu\text{Acm}^{-2}$. This is closer to the experimental and theoretical works [15, 7].

Density of the each particle solution is also given in this figure. Range of the solutions, values at the boundaries for each particle species are obtained same by each solver. However, these graphs are not similar especially at half interval of the region. This can be explained that accuracy of each method are different. COMSOL® uses FEM and Scharfetter Gummel method is semi implicit method. They are different from each other. Behaviours are similar but characters are different for each particle density graph. Methods that were used to obtain them cause this effect. Moreover, distribution of the mesh can cause this difference. On COMSOL®, mesh were distributed symmetrically intense at the boundary. This is a trick that is assumed the nonlinearity of the discharge appears especially at the boundaries. Thus, grid points exist intensively at the boundary. However, grid point interval on the MATLAB® code is constant and they are same for each interval. Mainly, distribution of the mesh points cause this difference.

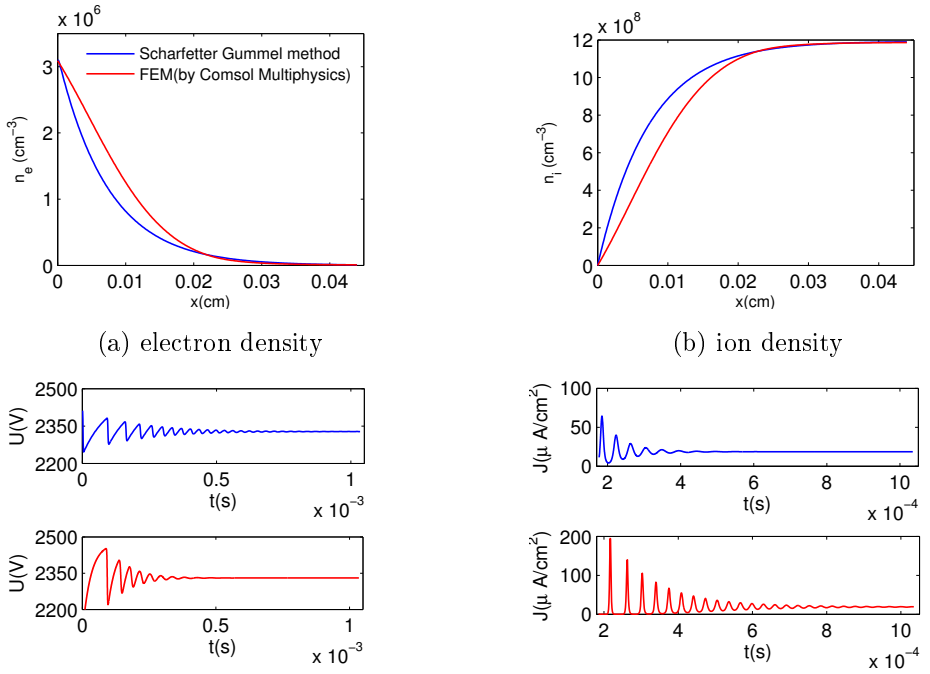

(a) electron density

(b) ion density

(c) voltage

(d) current

Figure 3.10: 1d solutions, (a)electron density, (b)ion density, (c)voltage, (d)current, applied voltage $U_t = 2473$ V

3.5 2D Analysis

In this part, 2d solutions are analysed. Three different cases are solved again to show effects. Each cases were resolved applying total voltage $U_t = 2397$ V and the remaining conditions are given in Table 2.3. In Figure 3.11, voltage values at the boundary point converges to the calculated breakdown voltage but current values are far from its characteristic value. Possible reasons are explained in the previous part.

Heat equation in the solutions was assumed to cause the nonlinearity of the system. It is not enough to show this effect in 1D solutions as shown in Figure 3.11. 2D solution gives more effective results for this nonlinearity since patterns distributes along x direction as shown in Figure 1.8.

In Figure 3.13, ion density and heat equation solutions are shown in 2D geometry. Patterns are seen there. It is interesting that change of the temperature value in a 20% causes this effect. This supports the explanation that is about the differece in solution of each cases in 1D. It was explained the differece between case 1 and 2 as changing the temperture value cause the differece on ion density graph. The gas temperature was taken constant in case 2.

In Figure 3.14, voltage, current and ion density vs x axis graphs are plotted. Each graph has an oscillating solution. They behaves similarly. Each one has seven main peak values along this boundary. Gas temperature affects the ion density since the diffusion coefficient of ion flux is proportional with the temperature value of the gas. Then, these patterns were obtained.

Solutions are consistent with the experimental results [15]. Patterns were observed in 2D solutions. Gas temperature is assumed to get these patterns [7]. Solutions are in agreement with the theoretical work [7].

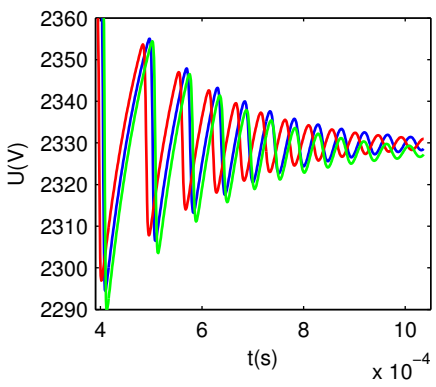

(a)

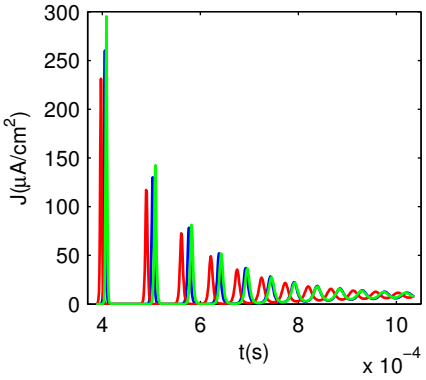

(b)

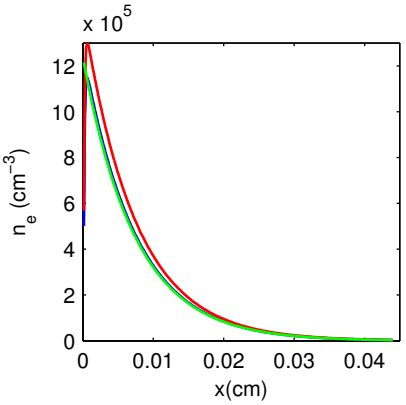

(c)

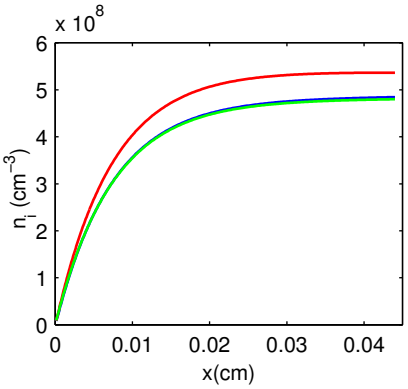

(d)

Figure 3.11: Solutions along normal to the electrodes, (a) voltage, (b) current, (c) ion density, (d) electron density, applied voltage $U_t = 2397$ V, remaining conditions are as given in Table 2.3.

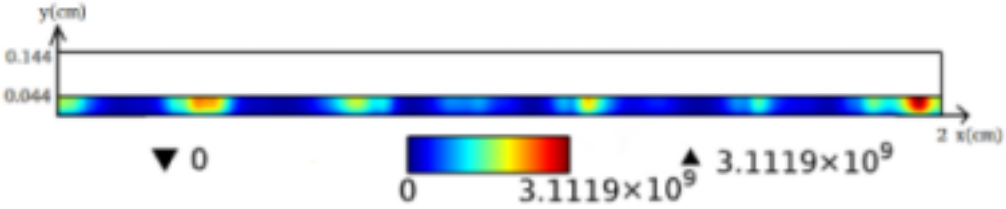

(a)

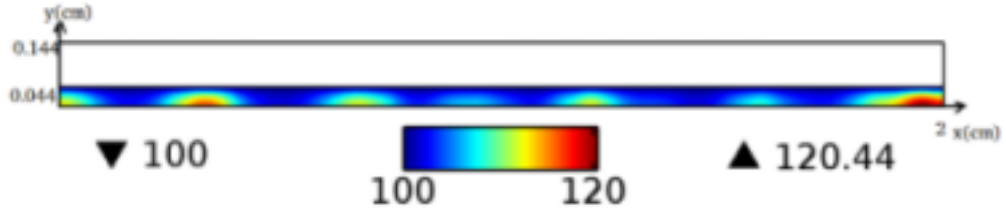

(b)

Figure 3.12: Patterns (a) ion density, (b) temperature, the same conditions as in figure 3.11.

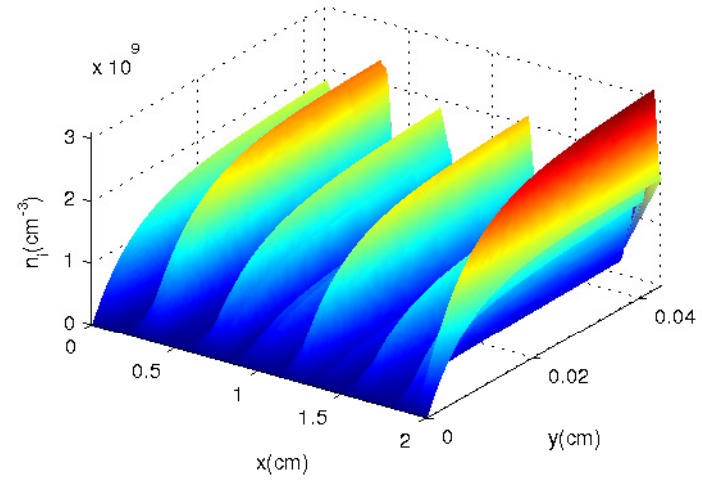

(a)

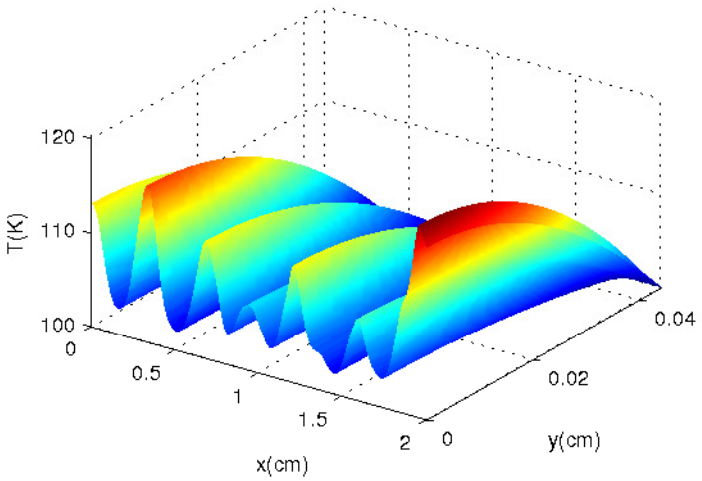

(b)

Figure 3.13: 2D solutions, (a) ion density, (b) gas temperature, applied voltage $U_t = 2397$ V, remaining conditions are given in Table 2.3.

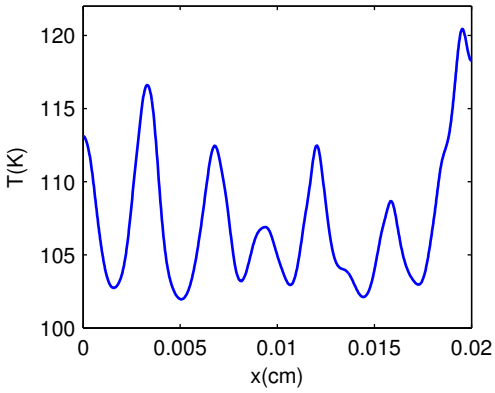

(a)

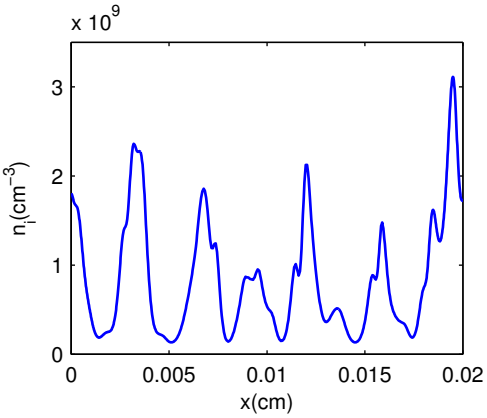

(b)

Figure 3.14: Solutions, (a) temperature along $y = 0$, (b) ion density $x = d_g$, applied voltage $U_t = 2397$ V, remaining conditions are as given in Table 2.3.

CHAPTER 4

CONCLUSION

In this thesis we have studied numerically the temporal and spatial pattern formation in the gas discharge- semiconductor (SC-GDG) system under experimental conditions [15] and [16]. This system consists of the planar gas discharge and high ohmic semiconductor layers, sandwiched between two planar electrodes, to which a DC potential is applied. The experimental conditions [15, 16] correspond to the transition from the Townsend regime to glow discharge. In these experiments, the nitrogen plasma is sustained at pressures 30 Torr [16] and 211.54 Torr [15], the gap size as well as the width of the semiconductor layer are of the order of 0.1 cm, the conductivities of the GaAs semiconductor are 3.85×10^{-6} $\Omega^{-1}\text{cm}^{-1}$ 1.3×10^{-8} $\Omega^{-1}\text{cm}^{-1}$, the temperature is 100 K.

Calculations are carried out in one and two spatial dimensions (1D,2D), using fluid equations of plasma in the drift-diffusion approximation. The models are derived within Comsol Multiphysics and Matlab computational packages.

First, within 1D model we studied the effects of different modelling approximations, namely

- effect of the diffusion flux,
- effect of heating of the background gas,
- effect of adiabatic elimination of the electron dynamics

on the computed results. Comparison of the solutions showed that in the considered parameter regime all these approximations lead nearly to the same results.

Next, we carried out 1D calculations under conditions of [16] and [15]. Results demonstrate the period doubling bifurcations of the system with increase in the applied voltage in exact agreement with [16]. Moreover, we developed the Lorenz diagrams, which indicate the transition of the system from periodic to chaotic regime as the applied voltage is increased. Then, Scharfetter Gummel method was used to solve the same system. Matlab was used to applied it. Nearly the same results with the other solution were obtained.

Finally, within 2D calculations under conditions [15] the spatial patterns were

obtained. Analysis confirm that computed results are in reasonable agreement with experimental observations and theoretical study [7].

REFERENCES

[1] Murray, J. (2003). *Mathematical Biology II Spatial Models and Biomedical Applications* (3rd ed.). Springer.

[2] Shang, W. (2007). *A Survey On Pattern Formation In DC Gas Discharge Systems* (Doctoral thesis,Institut für Angewandte Physik,Westfälische Wilhelms-Universität Münster). Retrieved from http://d-nb.info/985723483/34, (Last Access July 19, 2015).

[3] Ouellette, J. (2013, March 25). *Biologists Home in on Turing Patterns.* Retrieved from https://www.quantamagazine.org/20130325-biologists-home-in-on-turing-patterns/, (Last Access July 12, 2015).

[4] Turing, A. (1952). *The Chemical Basis Of Morphogenesis.* Philosophical Transactions of the Royal Society of London. Series B, Biological Sciences, **237(641)**, 37-72.

[5] Astrov, Y., Ammelt, E., Purwins, H., & Müller, I. (1998). Zigzag Destabilized Spirals and Targets. *Physical Review Letters*, **80(24)**.

[6] Raizer, Y. (1991). Gas Discharge Physics. Berlin: Springer-Verlag.

[7] Mokrov, M., & Raizer, Y. (2011). Simulation of current filamentation in a dc-driven planar gas discharge-semiconductor system. *Journal of Physics D: Applied Physics*, 44(425202).

[8] Strümpel, Y. A. Astrov, and H.-G. Purwins,*Phys. Rev. E* **62**, 4889 (2000).

[9] Boyers, D., & Tiller, W. (1982). *Plasma Bubble Domains: A magnetic Bubble Analog.* Applied of Physics, **41**, 28.

[10] Astrov, Y., Ammelt, E., Teperick, S., & Purwins, H. (1995). Hexagon and stripe Turing structures in a gas discharge system. *Physics Letters* A, **211**, 184-190.

[11] I. Rafatov, D. D. Sijacic and U. Ebert, *Phys. Rev. E* **76**, 036206 (2007).

[12] Astrov, Y., Ammelt, E., & Purwins, H. (1998). Hexagon structures in a two-dimensional dc-driven gas discharge system. *Physics Letters E*, **58(6)**.

[13] C. Strümpel, Y. A. Astrov, and H.-G. Purwins,*Phys. Rev. E* **63**, 026409 (2001).

[14] "Pattern Formation in Planar Dc Gas-discharge Systems." Retrieved from https://www.uni-muenster.de/Physik.AP/Purwins/DC/index-en.html (Last Access July 12, 2015,).

[15] Astrov, Y. A., Lodygin, A. N., & Portsel, L. M. Hexagonal Structures of Current in a "Semiconductor–Gas Discharge Gap" System. *Technical Physics*, **56**, 197-203.

[16] I. Rafatov, D. D. Sijacic and U. Ebert, *Phys. Rev. E* **70**, 056220 (2004)

[17] Astrov, Y. A. Formation of Clusters of Localized States in a Gas Discharge System via a Self-Completion Scenario. *Physical Review Letters*, **79**.

[18] Goldstone, R., & Rutherford, P. (2000). Introduction to Plasma Physics. New York: Taylor&Francis Group.

[19] E.van Groesen, J. Molenaar, Continuum Modeling in the Physical Sciences, SIAM, 2007.

[20] Strogatz, S. (1994). Nonlinear Dynamics And Chaos: With Applications To Physics, Biology, Chemistry, And Engineering. Persous Book Publishing.

[21] Mokrov, M., & Raizer, Y. (2010). A simple physical model of hexagonal patterns in a Townsend discharge with a semiconductor cathode. *Journal of Physics D: Applied Physics*, **43**.

[22] Lugiato, Luigi, Franco Prati, and Massimo Brambilla (2015), Nonlinear Optical Systems, Cambridge University Press.

[23] Liu, J. (n.d.). Scharfetter-Gummel Method. Retrieved from http://www.nhcue.edu.tw/ jinnliu/proj/Device/SGMethod.pdf, (Last Access June 22, 2015).

[24] Ammelt, E., Astrov, Y. A., & Purwins, H. Stripe Turing structures in a two-dimensional gas discharge system. *Physical Review E*, **55**.

[25] I. Rafatov, D. D. Sijacic and U. Ebert, *Phys. Rev. E* **71**, 066402 (2005).